Optimal Transmit Strategy for Multi-User MIMO WPT Systems With Non-Linear Energy Harvesters

Nikita Shanin, *Graduate Student Member, IEEE*, Laura Cottatellucci, *Member, IEEE*, and Robert Schober, *Fellow, IEEE*

***Abstract*— In this paper, we study multi-user multi-antenna wireless power transfer (WPT) systems, where each antenna at the energy harvesting (EH) nodes is connected to a dedicated non-linear rectifier. We propose optimal transmit strategies which maximize a weighted sum of the average harvested powers at the EH nodes subject to a constraint on the power budget of the transmitter. First, for multiple-input single-output (MISO) WPT systems, we prove that the optimal strategy employs maximum ratio transmission (MRT) beamforming and scalar symbols with arbitrary phases and discrete amplitudes following a probability density function (pdf) with at most two mass points. Then, we prove that for single-input multiple-output (SIMO) WPT systems, the optimal transmit symbol amplitudes are discrete random variables, whose pdf also has no more than two mass points. For general multi-user MIMO WPT, we show that the optimal transmit strategy employs scalar unit-norm symbols with arbitrary phases and at most two beamforming vectors. To determine these vectors, we formulate a non-convex optimization problem and obtain an optimal solution based on monotonic optimization. Since the computational complexity of the optimal solution is high, we propose a low-complexity iterative algorithm to obtain a suboptimal solution, which achieves near-optimal performance. Our simulation results reveal that the proposed transmit strategy for multi-user MIMO WPT systems outperforms baseline schemes based on a linear EH model and a single beamforming vector. For a given transmit power budget, we show that the harvested power saturates when increasing the number of transmit antennas. Finally, we observe that the harvested power region spanned by multiple EH nodes is convex and the power harvested at one EH node can be traded for a higher harvested power at the other nodes.**

***Index Terms*— Wireless power transmission, energy harvesting (EH), multiple-input multiple-output (MIMO), signal deisgn, rectennas, rectifiers.**

Manuscript received May 11, 2021; revised October 4, 2021 and November 8, 2021; accepted December 2, 2021. Date of publication December 10, 2021; date of current version March 17, 2022. This work was supported in part by the German Science Foundation through projects SCHO 831/12-1 and SFB 1483-Project-ID 442419336, EmpkinS. An earlier version of this paper was presented in part at the Biennial Symposium on Communications, Saskatoon, Canada, in 2021 [1] and in part at the IEEE 3rd International Workshop on Wirelessly Powered Systems and Networks, in 2021 [DOI: 10.1109/DCOSS52077.2021.00085]. The associate editor coordinating the review of this article and approving it for publication was B. Shim. *(Corresponding author: Nikita Shanin.)*

The authors are with the Institute for Digital Communications, Friedrich-Alexander-Universität (FAU) Erlangen-Nürnberg, 91058 Erlangen, Germany (e-mail: nikita.shanin@fau.de).

Color versions of one or more figures in this article are available at https://doi.org/10.1109/TCOMM.2021.3134690.

Digital Object Identifier 10.1109/TCOMM.2021.3134690

I. Introduction

THE device density in wireless communication networks has significantly increased over the past decades. The current trends for wireless systems suggest that the number of connected devices will continue to grow over the next few years and a longer battery life for these devices is highly desirable [3]. However, efficient charging of the batteries of wireless devices remains an unsolved problem. Since radio frequency (RF) signals are capable of transferring power, in recent years, far-field wireless power transfer (WPT) has attracted significant attention [4]–[24].

A typical WPT system comprises a transmitter (TX) that broadcasts an RF signal to energy harvesting (EH) nodes that collect the received power and deliver it to their respective loads, which store or consume the power, see Fig. 1 [4]. In fact, the harvested power can be stored in a battery [7] or utilized for sensing, signal processing, or information transmission tasks [8], [9]. In [5], the authors studied single-input single-output (SISO) WPT systems and showed that the power transferred to the EH node is maximized if a single sinusoidal signal is broadcasted by the TX. The authors of [6] extended these results to multiple-input multiple-output (MIMO) WPT systems and showed that the *input power* at the EH node is maximized if a scalar input symbol and *energy beamforming*, i.e., beamforming in the direction of the dominant eigenvector of the channel matrix, are employed at the TX. Although the solutions developed in [5] and [6] are optimal for the maximization of the power received by the EH node, they do not necessarily maximize the *harvested power* since practical EH circuits are non-linear [4], [10]–[12]. Hence, an accurate modeling of the EH circuit is crucial for the design of WPT systems [4], [10]–[24].

Practical EH nodes typically employ a rectenna, i.e., an antenna followed by a rectifier circuit that includes a non-linear element, namely, a diode. The experimental results reported in [10]–[12] show that rectennas exhibit a non-linear behaviour in both the low and high input power regimes. In particular, for low input power levels, the rectifier non-linearity is caused by the non-linear forward bias current-voltage characteristic of the diode [25], whereas in the high input power regime, practical EH circuits suffer from saturation due to the breakdown effect of the diode [26]. In order to capture these non-linearities, the authors in [11] modeled the

Fig. 1. WPT system comprising a TX, which is connected to a power source and broadcasts an RF signal, and an EH node that harvests the received RF power and delivers it to its load, which stores or consumes the harvested power.

harvested power as a parameterized sigmoidal function of the received power whose parameters depend on the waveform of the received signal. The model in [11] was widely utilized for the design of WPT [13], [14] and WPT-based communication systems [15]–[17]. In particular, in [13], it was shown that, adopting the EH model from [11], the energy beamforming proposed in [6] is also optimal for MIMO WPT systems. Furthermore, to avoid saturation of the rectenna circuits, based on the model in [11], the authors in [14] proposed to split the RF power received at the EH node between several collocated rectifiers.

Although the model in [11] characterizes the non-linear behavior of rectenna circuits, it is applicable only for signals with a known fixed waveform and does not allow the optimization of the waveform of the transmit signal [4]. Therefore, the authors in [18] proposed a non-linear EH model derived from the Taylor series expansion of the current flow through the rectifying diode of the EH node. Based on this model, the authors in [19] studied a WPT system with multiple antennas at the TX and a single antenna at the EH node, i.e., a multiple-input single-output (MISO) WPT system, and showed that the harvested power is maximized with energy beamforming [6], which reduces to scaled maximum ratio transmission (MRT) in this case. However, in [20], it was shown that energy beamforming is not optimal for general MIMO WPT systems employing non-linear rectenna circuits. In [21], the authors considered a MIMO WPT system, where the EH node is equipped with a single rectifier and proposed to combine the received signals of different antennas in the RF domain to increase the power at the input of the rectifier and, thus, maximize the harvested power. However, the practical implementation of the RF combining schemes considered in [14] and [21] requires complicated circuit designs and may also introduce associated losses, which are not desirable in practical systems [27]. Finally, the authors in [22] considered a MIMO WPT system, where each antenna of the EH node was equipped with a dedicated rectifier, and proposed an iterative algorithm to determine the TX beamforming vector that maximizes the weighted sum of powers harvested by the rectifiers.

Although the results in [18]–[22] provide important insights for the design of practical MIMO WPT systems, their applicability is limited to low input power levels at the EH node since the saturation of the harvested power is neglected in the underlying EH model [18]. A realistic EH model that accurately captures the rectenna non-linearity for both low and high input powers was developed in [23]. The analysis in [23] showed that for SISO WPT systems, it is optimal to adopt ON-OFF signaling at the TX, where the ON symbol and its probability are chosen to maximize the harvested power without saturating the EH node while satisfying an average power constraint at the TX. The optimality of ON-OFF signaling was confirmed in [24], where a learning-based approach was employed to model non-linear rectenna circuits equipped with a single and multiple diodes, respectively [26]. Finally, in [1] and [2], which are the conference versions of this paper, exploiting the rectenna model derived in [23], we studied the harvested power region of a two-user MISO WPT system and the maximum performance of a single-user MIMO WPT system, respectively. However, to the best of the authors' knowledge, the problem of optimizing the transmit strategy for multi-user MIMO WPT systems, where the EH nodes are equipped with multiple rectennas exhibiting non-linear behavior in both the low and high input power regimes, has not been solved, yet. We note that the EH model adopted in [1], [2] is a special case of the more general EH model considered in this paper. Hence, the results obtained for two-user MISO and single-user MIMO WPT systems in [1] and [2], respectively, are special cases of the results presented in this paper.

In this paper, we aim at determining the optimal transmit strategies for MISO, multi-user SIMO, and multi-user MIMO WPT systems, where each receive antenna is connected to a dedicated rectifier. In order to take the non-linearity of the EH node into account, we consider a general rectenna model characterized by a set of properties, which are typically satisfied for the practical rectenna circuits considered in the literature [4], [6], [11]–[14], [18]–[24]. Where appropriate, we specialize our results to the non-linear EH model proposed in [23]. We propose optimal transmit strategies, which are characterized by the distribution of the transmit symbol vector that maximizes a weighted sum of the average harvested powers at the EH nodes subject to a constraint on the power budget of the TX. The main contributions of this paper can be summarized as follows:

- For MISO WPT systems, we show that the optimal transmit strategy employs MRT beamforming and a scalar input symbol with an arbitrary phase and a discrete random amplitude following a probability density function (pdf) with at most two mass points. The optimal pdf of the symbol amplitudes is the solution of an optimization problem, which is solved via a two-dimensional grid search [28]. Furthermore, we show that for EH models, whose maximum harvested power is bounded, the optimal pdf exhibits an ON-OFF characteristic.
- For multi-user SIMO WPT systems, we show that the optimal transmit symbol amplitude is a discrete random variable, whose distribution has at most two mass points that can also be obtained by a two-dimensional grid search. Next, for SIMO WPT systems equipped with two rectennas, whose harvested power grows slower than quadratically with the input power, we show that the optimal distribution can be obtained in closed form and ON-OFF signaling is optimal if the power budget of the TX is low. Furthermore, for medium average transmit power budgets at the TX, the two discrete transmit symbol amplitudes are chosen such that one and both rectifiers are driven into saturation, respectively. Finally, for high average transmit power budgets, the optimal policy

is to saturate both rectifiers and the optimal pdf consists of a single mass point.

- For general MIMO WPT systems, we show that the optimal transmit strategy employs a scalar input symbol and at most two beamforming vectors, which can be determined as solution of a non-convex optimization problem. This optimal solution is obtained via monotonic optimization [29]. To reduce the high computational complexity of determining the optimal beamforming vectors, we develop a low-complexity iterative algorithm based on semi-definite relaxation (SDR) and successive convex approximation (SCA) to obtain a suboptimal solution. Our simulation results reveal that although the suboptimal solution for MIMO WPT systems has a much lower computational complexity than the optimal one, both solutions yield a similar performance.
- Our simulations show that the proposed MIMO WPT design outperforms baseline schemes based on the linear EH model in [6] and a single beamforming vector at the TX, respectively, at the expense of an increase in computational complexity. For the multi-user scenario and a given transmit power budget, we observe that the total average harvested power saturates when the TX is equipped with a large number of antennas. Finally, we observe that the harvested power region spanned by multiple EH nodes is convex and the average power harvested at one EH node can be traded for a higher harvested power at the other nodes.

The remainder of this paper is organized as follows. In Section II, we introduce the system model and discuss the adopted EH model. In Section III, we formulate an optimization problem for the maximization of the weighted sum of the average harvested powers at the EH nodes and establish a preliminary mathematical result needed for solving the problem. In Section IV, we determine the optimal transmit strategies for MISO, multi-user SIMO, and multi-user MIMO WPT systems, respectively. In Section V, we provide numerical results to evaluate the performance of the proposed designs. Finally, in Section VI, we draw some conclusions.

Notation: Bold upper case letters $\boldsymbol{X}$ represent matrices and $X_{i,j}$ denotes the element of $\boldsymbol{X}$ in row i and column j. Bold lower case letters $\boldsymbol{x}$ stand for vectors and x_i is the i^{th} element of $\boldsymbol{x}$. $\boldsymbol{X}^H$, $\text{Tr}\{\boldsymbol{X}\}$, and $\text{rank}\{\boldsymbol{X}\}$ denote the Hermitian, trace, and rank of matrix $\boldsymbol{X}$, respectively. The expectation with respect to random variable x is denoted by $\mathbb{E}_x\{\cdot\}$. The real part of a complex number is denoted by $\Re\{\cdot\}$. $\boldsymbol{x}^\top$ and $\|\boldsymbol{x}\|_2$ represent the transpose and L2-norm of $\boldsymbol{x}$, respectively. The imaginary unit is denoted by j. The sets of real, real non-negative, and complex numbers are denoted by $\mathbb{R}$, $\mathbb{R}_+$, and $\mathbb{C}$, respectively. $\mathbf{1}_K$ and $\mathbf{0}_K$ represent column vectors comprising K elements, where all elements are equal to 1 and 0, respectively. The Dirac delta function is denoted by $\delta(x)$. $f'(x_0)$ denotes the first-order derivative of function $f(x)$ evaluated at point $x = x_0$.

II. System Model and Preliminaries

In this section, we present the MIMO WPT system model and discuss the adopted multi-antenna EH model.

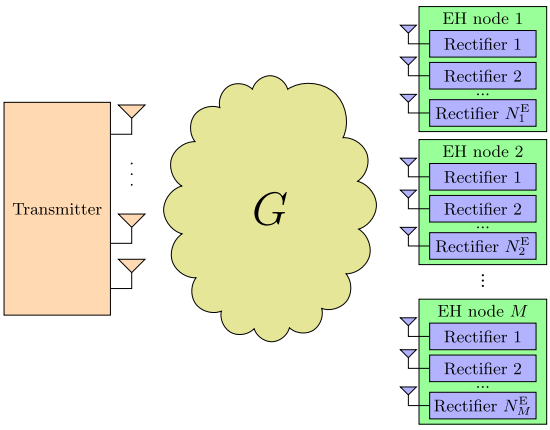

Fig. 2. Multi-user MIMO WPT system comprising a multi-antenna TX and M multi-antenna EH nodes, where node m, $m \in \{1, 2, \ldots, M\}$, is equipped with N_m^{E} rectennas followed by loads. Here, $\boldsymbol{G}$ denotes the channel between the TX and the EH nodes.

A. System Model

We consider a narrow-band multi-user MIMO WPT system comprising a TX with $N^{\text{T}} \geq 1$ antennas and M EH nodes, where EH node m, $m \in \{1, 2, \ldots, M\}$, is equipped with $N_m^{\text{E}} \geq 1$ antennas, see Fig. 2. The TX broadcasts a pulse-modulated RF signal, whose equivalent complex baseband (ECB) representation is modeled as $\boldsymbol{x}(t) = \sum_n \boldsymbol{x}[n]\psi(t-nT)$, where $\boldsymbol{x}[n] \in \mathbb{C}^{N^{\text{T}}}$ is the transmitted vector in time slot n, $\psi(t)$ is the transmit pulse with rectangular shape, and T is the symbol duration. Transmit vectors $\boldsymbol{x}[n]$ are mutually independent realizations of a random vector $\boldsymbol{x}$, whose probability density function (pdf) is denoted by $p_{\boldsymbol{x}}(\boldsymbol{x})$.

The ECB channel between the TX and antenna p of EH node m is characterized by row-vector $\boldsymbol{g}_p^m \in \mathbb{C}^{1\times N^{\text{T}}}$, $p \in \{1, 2, \ldots, N_m^{\text{E}}\}$. Thus, the RF signal received in time slot n at antenna p of EH node m is given by $z_{p,m}^{\text{RF}}(t) = \sqrt{2}\Re\{\boldsymbol{g}_p^m \boldsymbol{x}(t)\exp(j2\pi f_c t)\}$, where f_c denotes the carrier frequency. The noise received at the EH nodes is ignored since its contribution to the harvested energy is negligible.

The EH nodes are equipped with EH circuits that harvest the received RF power and deliver it to their respective loads, see Fig. 1. The power harvested at the EH nodes can be exploited by the load devices to perform, e.g., sensing, computation, and information transmission tasks, see [9], [16], [17]. In this paper, we assume that the TX is not aware of the ultimate use of the power harvested at the EH nodes. Thus, similar to [20]–[22], we focus exclusively on the optimal WPT. In the next section, we discuss the considered EH model in detail.

B. Energy Harvesting Model

In this paper, we assume that EH node m is equipped with N_m^{E} rectennas, i.e., each antenna is connected to a dedicated rectifier, see Fig. 2. Thus, the received ECB signal[1] at rectenna $p \in \{1, 2, \ldots, N_m^{\text{E}}\}$ of EH node m in time slot n is given by $z_p^m[n] = \boldsymbol{g}_p^m \boldsymbol{x}[n]$.

[1]We note that the EH nodes do not convert the RF signal into baseband. However, since the amount of the harvested power can be expressed as a function of the ECB signal received at the EH node, see, e.g., [19], [30], to simplify the notation, we use the ECB signal representation of the received RF signal.

Each rectenna comprises an antenna, a matching circuit, a non-linear rectifier with a low-pass filter, and a load resistor [4], [23], [24]. In order to maximize the power transferred to the rectifier, the matching circuit is typically well-tuned to the carrier frequency f_c and is designed to match the input impedance of the non-linear rectifier circuit with the output impedance of the antenna [31]. The rectifier is an electrical circuit that comprises a non-linear diode and a low-pass filter to convert the RF signal $z_{p,m}^{\mathrm{RF}}(t)$ received by rectenna p of EH node m to a direct current (DC) signal at the load resistor R_{L} of the rectenna.

In this paper, we make the following assumptions concerning the rectenna circuit.

Assumption 1: The rectenna circuit is memoryless, i.e., the amount of power harvested in time slot n depends on the ECB signal received in time slot n only.

Assumption 2: The harvested power depends on the magnitude of the received ECB signal only and is independent of its phase.

Assumption 3: The mapping between the received ECB signal z and the harvested power P_L is characterized by a non-linear and monotonically non-decreasing function[2] $P_L = \phi(|z|^2)$.

Assumption 1 is justified if the symbol duration T is sufficiently large. In this case, we can neglect the ripples of the voltage level across the load resistor R_{L} and the charging and discharging times of the reactive elements of the circuit. Thus, we can assume that the output voltage level of rectenna p of EH node m in time slot n is constant and depends only on the signal $z_p^m[n]$ [18], [23], [24]. Assumption 2 is justified since, for the considered narrow-band signals, the rectenna circuit behaves as an envelope detector [25] and, thus, its behavior is fully characterized by the magnitude $|z_p^m[n]|$ of the received ECB signal $z_p^m[n]$. Assumption 3 is satisfied since typical rectenna circuits include a diode that has a non-linear non-decreasing current-voltage characteristic [18], [23], [26].

Example: In this paper, as an example for an EH model that satisfies Assumptions 1-3, we adopt the model proposed in [23]. The corresponding power harvested by the rectenna as a function of the magnitude of the received ECB signal z is given as follows:

$$\phi(|z|^2) = \min\left\{\varphi(|z|^2), \varphi(A_s^2)\right\}, \tag{1}$$

where $\varphi(|z|^2) = \left[\frac{1}{a}W_0\left(a\exp(a)I_0\left(B\sqrt{2|z|^2}\right)\right) - 1\right]^2 I_s^2 R_L$, $a = \frac{I_s(R_L+R_s)}{\mu V_{\mathrm{T}}}$, $B = \frac{1}{\mu V_{\mathrm{T}}\sqrt{\Re\{1/Z_a^*\}}}$, and $W_0(\cdot)$ and $I_0(\cdot)$ are the principal branch of the Lambert-W function and the modified Bessel function of the first kind and zero order, respectively. Here, Z_a^*, V_{T}, I_s, R_s, and $\mu \in [1,2]$ are parameters of the rectenna circuit, namely, the complex-conjugate of the input impedance of the rectifier circuit, the thermal voltage, the reverse bias saturation current, the series resistance, and the ideality factor of the diode, respectively. These parameters depend on the circuit elements and are independent of the received signal. Finally, since for large input power levels, rectenna circuits are driven into saturation [11], [23], [24], [26], the function in (1) is bounded, i.e., $\phi(|z|^2) \leq \phi(A_s^2),\ \forall z \in \mathbb{C}$, where A_s is the minimum input signal magnitude level at which the output power starts to saturate.

[2]In this paper, to simplify the notation, we additionally assume that all electrical circuits equipped at the rectennas of the EH nodes are identical, i.e., all rectennas are characterized by the same function $\phi(\cdot)$. The generalization to the case, where the rectennas employ different electrical circuits, is straightforward.

III. Problem Formulation and Useful Result

In this section, we formulate an optimization problem for the maximization of the weighted average harvested power of the considered multi-user MIMO WPT system. Then, to obtain a preliminary result needed for solving this problem, we formulate and solve an auxiliary optimization problem, where we maximize the expected value of a function of a one-dimensional random variable under a constraint on its mean value.

A. Problem Formulation

We characterize the transmit strategy via the pdf $p_{\boldsymbol{x}}(\boldsymbol{x})$ of transmit symbol vector $\boldsymbol{x}$. The objective of the proposed transmit strategy is to maximize the weighted average power harvested at the EH nodes under an average power constraint at the TX. Thus, we formulate the following optimization problem:

$$\underset{p_{\boldsymbol{x}}}{\text{maximize}}\ \ \overline{\Phi}(p_{\boldsymbol{x}}) \tag{2a}$$

$$\text{subject to}\ \ \int_{\boldsymbol{x}} \|\boldsymbol{x}\|_2^2\, p_{\boldsymbol{x}}(\boldsymbol{x})d\boldsymbol{x} \leq P_x, \tag{2b}$$

$$\int_{\boldsymbol{x}} p_{\boldsymbol{x}}(\boldsymbol{x})d\boldsymbol{x} = 1, \tag{2c}$$

where the objective function is the weighted sum of the average harvested powers at the EH nodes defined as

$$\overline{\Phi}(p_{\boldsymbol{x}}) = \sum_{m=1}^{M} \xi_m \mathbb{E}_{\boldsymbol{x}}\left\{\psi_m(\boldsymbol{x})\right\}. \tag{3}$$

Here, $\psi_m(\boldsymbol{x}) = \sum_{p=1}^{N_m^{\mathrm{E}}} \phi(|\boldsymbol{g}_p^m \boldsymbol{x}|^2)$ is the total power harvested by EH node m and $\xi_m \geq 0, m \in \{1,2,\ldots,M\}$, $\sum_m \xi_m = 1$, is the weight for EH node m [21]. We note that the weights associated with the users allow the TX to control the distribution of the harvested power among the EH nodes. In particular, if weight ξ_m is increased, the optimal transmit strategy will favor EH node m and increase the average harvested power $\mathbb{E}\{\psi_m(\boldsymbol{x})\}$ at EH node m at the expense of the average harvested powers at the other EH nodes. Furthermore, we impose constraints (2b) and (2c) to limit the transmit power budget at the TX and ensure that $p_{\boldsymbol{x}}(\boldsymbol{x})$ is a valid pdf, respectively.

Remark 1: Optimization problem (2) may have an infinite number of solutions. In particular, for a general EH model satisfying Assumptions 1 - 3, since $\|\boldsymbol{x}\|_2$ and the average harvested power $\overline{\Phi}(\cdot)$ are invariant under phase rotation of the transmit symbol vector $\boldsymbol{x}$, given an optimal pdf $p_{\boldsymbol{x}}^*(\boldsymbol{x})$ and a random phase $\phi_x \in [-\pi, \pi)$ with an arbitrary pdf $p_{\phi_x}(\phi_x)$, the

random vector $\tilde{\boldsymbol{x}} = \exp(j\phi_x)\boldsymbol{x}$ is still a solution of (2) [24]. Furthermore, we note that, for bounded $\phi(\cdot)$, such as (1), if affordable by the power budget P_x, there may be an infinite number of pdfs that drive all the rectifiers of the EH node into saturation while satisfying constraints (2b) and (2c). Thus, in the following, we determine one pdf $p^*_{\boldsymbol{x}}(\boldsymbol{x})$ that solves (2).

Before tackling problem (2), we first consider a related auxiliary optimization problem. In the next subsection, we formulate and solve this auxiliary problem, namely, the maximization of the expectation of a non-decreasing function $f(\nu)$ of a scalar random variable ν under a constraint on the mean value of ν.

B. Auxiliary Optimization Problem

In this section, we study an auxiliary optimization problem, whose solution will be leveraged in Section IV for solving problem (2). Let us consider the following optimization problem:

$$\underset{p_\nu}{\text{maximize}}\ \mathbb{E}_\nu\{f(\nu)\} \quad \text{subject to}\ \mathbb{E}_\nu\{\nu\} \le A_\nu, \tag{4}$$

whose solution is the pdf $p_\nu(\nu)$ which maximizes the expectation of $f(\nu)$ under a constraint on the mean value of ν. In order to solve (4), let us first define the slope of the straight line connecting points $\big(\nu_1, f(\nu_1)\big)$ and $\big(\nu_2, f(\nu_2)\big)$, where $\nu_2 > \nu_1$, as follows:

$$\sigma(\nu_1, \nu_2; f) = \frac{f(\nu_2) - f(\nu_1)}{\nu_2 - \nu_1}. \tag{5}$$

Then, we establish an upper-bound on $\mathbb{E}_\nu\{f(\nu)\}$. We note that if $f(\nu)$ is convex (concave), an upper-bound on $\mathbb{E}_\nu\{f(\nu)\}$ is given by the Edmundson-Madansky (Jensen's) inequality, e.g., [32]. However, since we intend to apply this result to the weighted sum of functions $\psi_m(\cdot), m \in \{1, 2, \ldots, M\}$, in (2), which are not necessarily convex or concave, in the following lemma, we extend the Edmundson-Madansky and Jensen's inequalities to arbitrary non-decreasing functions $f(\nu)$ and determine an upper-bound on the expectation of $f(\nu)$.

Lemma 1: Let us consider a non-decreasing function $f(\nu)$ of random variable ν. Then, for a given mean value of ν, $\overline{\nu} = \mathbb{E}_\nu\{\nu\}$, the expectation of $f(\nu)$ is upper-bounded by the following inequality:

$$\mathbb{E}_\nu\{f(\nu)\} \le E_f\big(\overline{\nu}\big), \tag{6}$$

where $E_f(\overline{\nu}) = \beta f(\nu_1^*) + (1-\beta) f(\nu_2^*)$ and $\beta = \frac{\nu_2^* - \overline{\nu}}{\nu_2^* - \nu_1^*}$. Here, ν_1^* and ν_2^* are given by $\nu_1^* = \arg\min_{\nu_1 \le \overline{\nu}} \gamma(\nu_1; f)$, where $\gamma(\nu_1; f) = \max_{\nu_2 \ge \overline{\nu}} \sigma(\nu_1, \nu_2; f)$, and $\nu_2^* = \arg\max_{\nu_2 \ge \overline{\nu}} \sigma(\nu_1^*, \nu_2; f)$, respectively. Furthermore, inequality (6) holds with equality if the pdf of ν is given by $p^*_\nu(\nu) = \beta\delta(\nu - \nu_1^*) + (1-\beta)\delta(\nu - \nu_2^*)$.

Proof: Please refer to Appendix VI. ∎

Lemma 1 implies that for any non-decreasing function $f(\nu)$ of random variable ν, an upper bound on the expectation of $f(\nu)$ is given by (6). Furthermore, a discrete pdf, $p_\nu(\nu)$, with no more than two mass points, whose values ν_1^* and ν_2^* are obtained as the solutions of a min-max optimization problem, is sufficient to attain this upper bound. In the following corollary, we show that for a certain class of functions $f(\nu)$, the result in Lemma 1 can be significantly simplified.

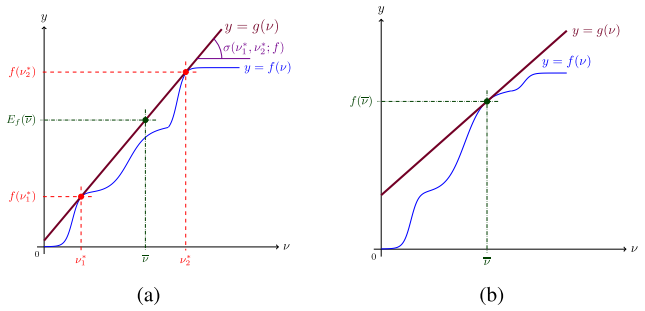

Fig. 3. Illustrations of Lemma 1 and Corollary 1.

Corollary 1: Let us consider a non-decreasing function $f(\nu)$ of random variable ν. If function $f(\cdot)$ is differentiable at $\overline{\nu} = \mathbb{E}_\nu\{\nu\}$ and the following property holds:

$$f'(\overline{\nu})(\overline{\nu} - \nu) \le f(\overline{\nu}) - f(\nu), \quad \forall \nu \in \mathbb{R}, \tag{7}$$

then the expectation of $f(\nu)$ is upper-bounded by $\mathbb{E}_\nu\{f(\nu)\} \le f\big(\overline{\nu}\big)$, where the inequality holds with equality if the pdf of ν is given by $p^*_\nu(\nu) = \delta(\nu - \overline{\nu})$.

Proof: Please refer to Appendix VI. ∎

We note that $E_f\big(\mathbb{E}_\nu\{\nu\}\big)$ in Lemma 1 can be interpreted as the value of linear function $g(\nu)$, defined by points $\big(\nu_1^*, f(\nu_1^*)\big)$ and $\big(\nu_2^*, f(\nu_2^*)\big)$, at $\overline{\nu} = \mathbb{E}_\nu\{\nu\}$, where the choice of ν_1^* and ν_2^* ensures that $g(\nu) \ge f(\nu)$, $\forall \nu \in \mathbb{R}$, see Fig. 3(a). However, if condition (7) in Corollary 1 is satisfied, points ν_1^* and ν_2^* coincide, i.e., $\nu_1^* = \lim_{\epsilon \to 0} \overline{\nu} - \epsilon$ and $\nu_2^* = \lim_{\epsilon \to 0} \overline{\nu} + \epsilon$, and then, $g(\nu) = f(\overline{\nu}) + f'(\overline{\nu})(\nu - \overline{\nu}) \ge f(\nu)$, $\forall \nu \in \mathbb{R}$, see Fig. 3(b).

Finally, exploiting Lemma 1 and Corollary 1, in the following corollary, we determine the optimal pdf $p^*_\nu(\nu)$ of random variable ν solving optimization problem (4).

Corollary 2: A solution[3] of optimization problem (4) is a discrete pdf given by $p^*_\nu(\nu) = \delta(\nu - A_\nu)$ if condition (7) holds, and $p^*_\nu(\nu) = \beta\delta(\nu - \nu_1^*) + (1-\beta)\delta(\nu - \nu_2^*)$, where $\nu_1^* = \arg\min_{\nu_1 \le A_\nu} \gamma(\nu_1; f)$, $\gamma(\nu_1; f) = \max_{\nu_2 \ge A_\nu} \sigma(\nu_1, \nu_2; f)$, $\nu_2^* = \arg\max_{\nu_2 \ge A_\nu} \sigma(\nu_1^*, \nu_2; f)$, $\beta = \frac{\nu_2^* - A_\nu}{\nu_2^* - \nu_1^*}$, otherwise.

Proof: Please refer to Appendix VI. ∎

The results in Lemma 1, Corollary 1, and Corollary 2 will be exploited in Section IV for solving the transmit strategy optimization problem in (2).

IV. Optimal Transmit Strategies

In this section, we first consider MISO and SIMO WPT systems, where the EH node and the TX are equipped with a single antenna, respectively. For each system architecture, we determine the optimal pdf $p^*_{\boldsymbol{x}}(\boldsymbol{x})$ that solves (2) and the corresponding optimal transmit strategy. Then, we consider the general multi-user MIMO WPT case, characterize the solution of (2), and present optimal and suboptimal transmit strategies.

[3]We note that, similar to (2), problem (4) may have an infinite number of solutions, i.e., for a given monotonic non-decreasing function $f(\cdot)$, there may exist multiple pdfs $p_\nu(\nu)$ that yield the same value of $\mathbb{E}_\nu\{f(\nu)\}$ and satisfy the constraint in (4). In Corollary 2, we obtain one solution of (4).

A. MISO WPT Systems

In the following, we consider MISO WPT systems employing a single-antenna EH node, i.e., $M = N_1^{\mathrm{E}} = 1$, and a TX equipped with $N^{\mathrm{T}} \geq 1$ antennas. In this case, the weighted sum in (3) reduces to $\overline{\Phi}(p_{\boldsymbol{x}}) = \mathbb{E}_{\boldsymbol{x}}\{\phi(|\boldsymbol{g}\boldsymbol{x}|^2)\}$, where $\boldsymbol{g}$ is the row-vector representing the channel between the TX and the EH node. In the following proposition, we provide a solution of optimization problem (2) for MISO WPT systems and the corresponding optimal transmit strategy.

Proposition 1: For MISO WPT systems, function $\overline{\Phi}(\cdot)$ is maximized by transmit vectors $\boldsymbol{x} = \boldsymbol{w}s$, where $\boldsymbol{w} = \frac{\boldsymbol{g}^H}{\|\boldsymbol{g}\|_2}$ is the MRT beamforming vector and $s = r_s \exp(j\theta_s)$ is a scalar random symbol with arbitrary phase θ_s and amplitude r_s following distribution $p^*_{r_s}(r_s)$. Furthermore, for the optimal transmit strategy, the pdf of the symbol amplitudes r_s is given by $p^*_{r_s}(r_s) = \delta(r_s - \sqrt{P_x})$ if the following inequality holds:

$$\Phi'(P_x)\big(P_x - r_s^2\big) \leq \Phi(P_x) - \Phi(r_s^2), \quad \forall r_s \in \mathbb{R}_+, \tag{8}$$

where $\Phi(r^2) = \phi\big(r^2\|\boldsymbol{g}\|_2^2\big)$. If (8) does not hold, the optimal transmit strategy is characterized by pdf $p^*_{r_s}(r_s) = (1-\beta)\delta(r_s - \sqrt{\nu_1^*}) + \beta\delta(r_s - \sqrt{\nu_2^*})$, where $\beta = \frac{\nu_2^* - P_x}{\nu_2^* - \nu_1^*}$. Here, ν_1^* and ν_2^* are the solutions of the following min-max optimization problem:

$$\nu_1^* = \underset{\nu_1 \leq P_x}{\arg\min}\, \gamma(\nu_1; \Phi) \tag{9}$$

with $\gamma(\nu_1;\Phi) = \max_{\nu_2 \geq P_x} \sigma(\nu_1, \nu_2; \Phi)$ and $\sigma(\nu_1, \nu_2; \Phi) = \frac{\Phi(\nu_2) - \Phi(\nu_1)}{\nu_2 - \nu_1}$ and

$$\nu_2^* = \underset{\nu_2 \geq P_x}{\arg\max}\, \sigma(\nu_1^*, \nu_2; \Phi), \tag{10}$$

respectively.

Proof: Please refer to Appendix VI. ∎

Proposition 1 reveals that, as for linear EH nodes in [6], for the considered non-linear EH model, MRT beamforming is optimal. Furthermore, similar to the SISO case in [23], for MISO WPT systems, there exists an optimal input symbol amplitude that follows a discrete pdf, $p^*_{r_s}(r_s)$, consisting of at most two mass points. In particular, it is optimal to adopt a single sinusoidal signal s with amplitude $r_s = \sqrt{P_x}$ and an arbitrary phase θ_s if condition (8) holds. If (8) does not hold, amplitude r_s is a discrete binary random variable. In this case, in order to obtain the pdf $p^*_{r_s}(r_s)$, the non-convex min-max optimization problem defined by (9), (10) has to be solved. Due to the low dimensionality of the problem, we propose to obtain the optimal solution via a two-dimensional grid search [28].

1) Grid Search Method: In the following, we propose a grid-search based method for solving the min-max optimization problem in Proposition 1. We note that this problem is not convex since function $\sigma(\nu_1, \nu_2; \Phi)$ is not convex and not concave in ν_1 and ν_2, respectively. However, since the dimensionality of the problem is low, performing a grid search to determine ν_1^* and ν_2^* entails limited and affordable complexity [28]. To this end, we define a uniform grid $\mathcal{P} = \{\rho_0, \rho_1, \rho_2, \ldots, \rho_{N_\rho}\}$, where $\rho_0 = 0$, $\rho_j = \Delta_\rho + \rho_{j-1}$, $j = 1, 2, \ldots, N_\rho$, N_ρ is the grid size, and Δ_ρ is a predefined step size. Then, we define the smallest element of $\mathcal{P}$ which is larger than P_x as ρ_n, i.e., $\rho_n = \min\{\rho_j | \rho_j \geq P_x, j = 0, 1, \ldots, N_\rho\}$. Next, we define a matrix $\boldsymbol{S} \in \mathbb{R}^{n \times (N_\rho - n + 1)}$, whose elements are the values of function $\sigma(\cdot, \cdot; \Phi)$ evaluated at the elements of $\mathcal{P}$, i.e., $S_{i,j} = \sigma(\rho_i, \rho_{j'}; \Phi)$, $i = 0, 1, \ldots, n-1$, $j = j' - n$, and $j' = n, n+1, \ldots, N_\rho$. Finally, we obtain the power values $\nu_1^* = \rho_{i^*}$ and $\nu_2^* = \rho_{n+j^*}$, where $i^* = \arg\min_i \max_j S_{i,j}$ and $j^* = \arg\max_j S_{i^*,j}$, respectively. The proposed grid-search method is summarized in Algorithm 1. The computational complexity of Algorithm 1 is quadratic with respect to the grid size N_ρ and does not depend on the number of TX antennas N^{T}.

Algorithm 1 Grid Search for Determining the Optimal Values ν_1^*, ν_2^*, and β

Initialize: Grid size N_ρ, step size Δ_ρ, maximum TX power P_x, initial value $\rho_0 = 0$.

1. Compute the grid $\mathcal{P}$ and the values of $\Phi(\cdot)$ for the grid elements:

for $m = 0$ to N_ρ **do**

1.1. Compute $\Phi_m = \Phi(\rho_m)$

1.2. Set $\rho_{m+1} = \rho_m + \Delta_\rho$

end

2. Determine grid element

$\rho_n = \min\{\rho_j | \rho_j \geq P_x, j = 0, 1, \ldots, N_\rho\}$

3. Calculate the elements of matrix $\boldsymbol{S}$ as

$S_{i,j} = \sigma(\rho_i, \rho_{j'}; \Phi) = \frac{\Phi_{j'} - \Phi_i}{\rho_{j'} - \rho_i}$, $i = 0, 1, \ldots, n-1$, $j = j' - n$, and $j' = n, n+1, \ldots, N_\rho$

4. Determine power values $\nu_1^* = \rho_{i^*}$ and $\nu_2^* = \rho_{n+j^*}$, where $i^* = \arg\min_i \max_j S_{i,j}$ and $j^* = \arg\max_j S_{i^*,j}$

Output: Optimal values ν_1^*, ν_2^*, $\beta = \frac{\nu_2^* - P_x}{\nu_2^* - \nu_1^*}$

2) Special Case: In the following, we consider the special case of MISO WPT systems, where the EH model satisfies the following additional assumption.

Assumption 4: For the EH model $\phi(\cdot)$, there is a value A_s, such that $\forall z : |z| \leq A_s$, $\phi(|z|^2)$ is a convex function and $\forall z : |z| > A_s$, $\phi(|z|^2) = \phi(A_s^2)$.

In particular, we note that Assumption 4 holds for the EH model in (1). In the following corollary, we show that for an EH model satisfying Assumption 4, the result in Proposition 1 can be significantly simplified.

Corollary 3: For an EH model satisfying Assumption 4, the pdf $p^*_{r_s}(r_s)$ of the transmit symbol amplitudes r_s in Proposition 1 is given by $p^*_{r_s}(r_s) = \delta(r_s - \sqrt{P_x^{\max}})$ if $P_x \geq P_x^{\max} = \frac{A_s^2}{\|\boldsymbol{g}\|_2^2}$ and $p^*_{r_s}(r_s) = (1-\beta)\delta(r_s) + \beta\delta(r_s - \sqrt{P_x^{\max}})$, where $\beta = \frac{P_x^{\max} - P_x}{P_x^{\max}}$, otherwise.

Proof: First, we note that $\forall \nu \in \mathbb{R}_+$, $\Phi(\nu) \leq \Phi(P_x^{\max}) = \phi(A_s^2)$. Therefore, for $P_x \geq P_x^{\max}$, the optimal transmit strategy is characterized by the pdf $p^*_{r_s}(r_s) = \delta(r_s - \sqrt{P_x^{\max}})$. Furthermore, functions $\phi(|z|^2)$ in (1) and $\Phi(\nu)$ in

Proposition 1 are convex and increasing in the intervals $|z|^2 \in [0, A_s^2]$ and $\nu \in [0, P_x^{\max}]$, respectively. Hence, $\forall P_x : P_x < P_x^{\max}$, due to the convexity of $\Phi(\nu)$, the solutions of the optimization problems in Proposition 1 are given by $\nu_1^* = 0$ and $\nu_2^* = P_x^{\max}$, respectively, with $\beta = \frac{P_x^{\max} - P_x}{P_x^{\max}}$. This concludes the proof. ∎

Corollary 3 reveals that if $P_x < P_x^{\max}$, ON-OFF signaling with MRT beamforming is optimal, which is similar to the result obtained for SISO WPT systems in [23]. Furthermore, for $P_x \geq P_x^{\max}$, it is affordable to drive the EH node into saturation and, hence, the optimal pdf of r_s consists of a single mass point. We note that in contrast to Proposition 1, where the entire power budget P_x is utilized for the transmission, Corollary 3 shows that for EH models satisfying Assumption 4 and $P_x \geq P_x^{\max}$, there is an optimal transmit strategy, where the average transmit power is equal to $P_x^{\max}$.

B. SIMO WPT Systems

In the following, we consider a SIMO WPT system, where M EH nodes are equipped with $N_m^{\mathrm{E}} \geq 1$, $m \in \{1, 2, \ldots, M\}$, antennas and the TX has a single antenna, i.e., $N^{\mathrm{T}} = 1$. In this case, as in [23], [24], due to Assumption 2, the powers harvested at the rectennas depend on the magnitude of the scalar transmit symbol but not on its phase. Hence, the weighted sum in (3) can be expressed as a function of the pdf p_{r_x} of the transmit symbol amplitude $r_x = |x|$ as follows $\overline{\Phi}(p_{r_x}) = \mathbb{E}_{r_x}\{\Phi(r_x^2)\}$, where

$$\Phi(r_x^2) = \sum_{m=1}^{M} \sum_{p=1}^{N_m^{\mathrm{E}}} \xi_m \phi(r_x^2 |g_p^m|^2) \tag{11}$$

and $|g_p^m|$ is the magnitude of the scalar channel coefficient g_p^m between the transmit antenna and antenna p of EH node m. In the following proposition, we provide a solution of optimization problem (2) for SIMO WPT systems and the corresponding optimal transmit strategy.

Proposition 2: For the considered SIMO WPT system, function $\overline{\Phi}(\cdot)$ is maximized for discrete transmit symbol amplitudes following distribution $p_{r_x}^*(r_x)$. In particular, the optimal transmit strategy is characterized by the pdf $p_{r_x}^*(r_x) = \delta(r_x - \sqrt{P_x})$, if function $\Phi(r_x^2)$ is differentiable at $r_x^2 = P_x$ and the following inequality holds:

$$\Phi'(P_x)\big(P_x - r_x^2\big) \leq \Phi(P_x) - \Phi(r_x^2), \quad \forall r_x \in \mathbb{R}_+. \tag{12}$$

Furthermore, if (12) does not hold, the optimal pdf is given by $p_{r_x}^*(r_x) = \beta\delta(r_x - \sqrt{\nu_1^*}) + (1-\beta)\delta(r_x - \sqrt{\nu_2^*})$, where $\beta = \frac{\nu_2^* - P_x}{\nu_2^* - \nu_1^*}$. Here, ν_1^* and ν_2^* are the corresponding solutions of the optimization problems in (9) and (10), respectively, where function $\Phi(\cdot)$ is given by (11).

Proof: Please refer to Appendix VI. ∎

Proposition 2 reveals that there exists an optimal pdf $p_{r_x}^*(r_x)$ of the symbol amplitudes r_x that is discrete and consists of one or two mass points. In particular, as for SISO and MISO WPT systems in [5] and in Section IV-A, respectively, it is optimal to transmit a single sinusoid if condition (12) holds. If (12) does not hold, this optimal pdf consists of two mass points, ν_1^* and ν_2^*, which are obtained as solutions of the min-max optimization problem (9), (10). Due to its low dimensionality, this problem also can be efficiently solved via a two-dimensional grid search, as discussed in Section IV-A.1 and summarized in Algorithm 1. Thus, the computational complexity of determining the optimal transmit strategy for SIMO WPT systems is independent of the number of EH nodes M and the number of antennas N_m^{E} at each EH node $m \in \{1, 2, \ldots, M\}$.

Special Case: In the following, we consider the special case of SIMO WPT systems, where the EH model satisfies the following additional assumption.

Assumption 5: For function $\phi(\cdot)$, Assumption 4 is satisfied. Furthermore, for the value A_s, $\forall z : |z| \leq A_s$, the following inequality holds: $\phi(|z|^2) \geq \phi(A_s^2)\Big(\frac{|z|^2}{A_s^2}\Big)^2$.

We note that the condition in Assumption 5 implies that the power harvested by the rectifier grows slower than quadratically with the input power. In particular, it can be shown that Assumption 5 is satisfied for the EH model in (1). Let us now consider a SIMO WPT system with two rectifiers, i.e., $M = 1$ and $N_1^{\mathrm{E}} = 2$ or $M = 2$ and $N_1^{\mathrm{E}} = N_2^{\mathrm{E}} = 1$. In this case, without loss of generality, we denote the scalar channel coefficients between the transmit antenna and the antennas of the rectifiers by g_1 and g_2 and assume that $|g_1| \geq |g_2|$. Then, in the following corollary, we provide a closed form solution for the optimal ν_1^* and ν_2^* in Proposition 2.

Corollary 4: Let us consider a SIMO WPT system with two rectifiers and an EH model satisfying Assumption 5. In this case, if $P_x < \rho_{\min} = \frac{A_s^2}{|g_1|^2}$, the optimal transmit strategy is characterized by the pdf of the transmit symbol amplitudes given by $p_{r_x}^*(r_x) = \beta\delta(r_x) + (1-\beta)\delta(r_x - \sqrt{\rho_{\min}})$, where $\beta = \frac{\rho_{\min} - P_x}{\rho_{\min}}$. Furthermore, if $P_x \in [\rho_{\min}, \rho_{\max})$, where $\rho_{\max} = \frac{A_s^2}{|g_2|^2}$, then $p_{r_x}^*(r_x) = \beta\delta(r_x - \sqrt{\rho_{\min}}) + (1-\beta)\delta(r_x - \sqrt{\rho_{\max}})$ with $\beta = \frac{\rho_{\max} - P_x}{\rho_{\max} - \rho_{\min}}$. Finally, if $P_x \geq \rho_{\max}$, the pdf is given by $p_{r_x}^*(r_x) = \delta(r_x - \sqrt{\rho_{\max}})$.

Proof: Please refer to Appendix VI. ∎

Thus, for SIMO WPT systems with two rectifiers, if the transmit power budget is low, i.e., $P_x < \rho_{\min}$, similar to the SISO and MISO WPT cases, ON-OFF signaling is optimal, where the ON signal drives the rectifier with the best channel conditions into saturation. Furthermore, for $P_x \in [\rho_{\min}, \rho_{\max})$, the pdf $p_{r_x}^*(r_x)$ has two mass points, which are chosen to drive one and both rectifiers into saturation, respectively. For $P_x \geq \rho_{\max}$, it is affordable to drive both rectifiers into saturation and, hence, the optimal pdf consists of a single mass point. Moreover, as for MISO WPT systems, Corollary 4 reveals that for $P_x \geq \rho_{\max}$, the average transmit power of the optimal transmit strategy is equal to $\rho_{\max}$.

C. MIMO WPT Systems

In the following, we consider the general multi-user MIMO WPT system in Fig. 2, where $N^{\mathrm{T}} \geq 1$ and $N_m^{\mathrm{E}} \geq 1$ antennas are employed at the TX and EH node m, $m \in \{1, 2, \ldots, M\}$, respectively. For these systems, exploiting Corollary 2, we first show that for the optimal solution of (2), at most two beamforming vectors are needed at the TX. Next, in order to determine these beamforming vectors, we use the monotonic

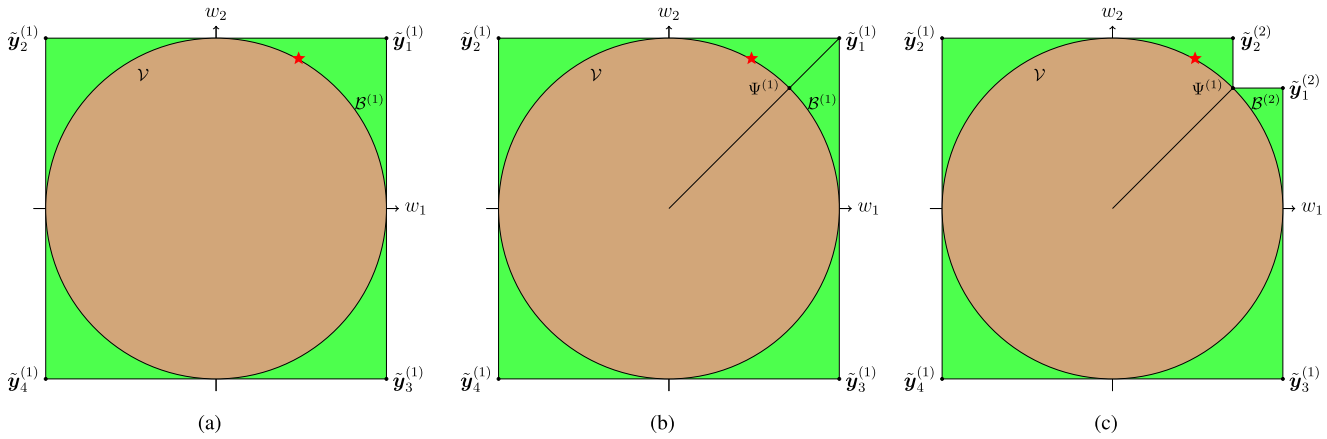

Fig. 4. Illustration of the polyblock optimization approach. The red star is the optimal point on the feasible set $\mathcal{V}$.

polyblock optimization framework in [29]. Finally, since the computational complexity of the optimal scheme is high, we also propose a suboptimal iterative algorithm based on SDR and SCA to obtain the beamforming vectors [33]–[35].

In the following proposition, we characterize a solution of (2) and the corresponding optimal transmit strategy.

Proposition 3: For multi-user MIMO WPT systems, function $\overline{\Phi}(\cdot)$ *is maximized for discrete random transmit symbol vectors* $\boldsymbol{x} = \boldsymbol{w}s$*, where* $s = \exp(j\theta_s)$ *is a unit-norm symbol with an arbitrary phase* θ_s*. Here,* $\boldsymbol{w}$ *is a discrete random beamforming vector, whose pdf is given by* $p^*_{\boldsymbol{w}}(\boldsymbol{w}) = \beta\delta(\boldsymbol{w}-\boldsymbol{w}_1^*) + (1-\beta)\delta(\boldsymbol{w}-\boldsymbol{w}_2^*)$*. The beamforming vectors* $\boldsymbol{w}_n^*, n \in \{1,2\}$*, are given by*

$$\boldsymbol{w}_n^* \in \{\boldsymbol{w} : \Psi(\boldsymbol{w}) = \Phi(\nu_n^*)\}, \tag{13}$$

$$\Phi(\nu) = \max_{\{\boldsymbol{w}\,|\,\boldsymbol{w}\in\mathbb{C}^{N^{\mathrm{T}}},\,\|\boldsymbol{w}\|_2^2=\nu\}} \Psi(\boldsymbol{w}), \tag{14}$$

where $\Psi(\boldsymbol{x}) = \sum_m \xi_m \psi_m(\boldsymbol{x})$*. Here,* ν_1^* *and* ν_2^* *are the corresponding solutions of the optimization problems in (9) and (10), respectively, where* $\Phi(\cdot)$ *is given by (14). Furthermore, if the following inequality holds*:

$$\Phi'(P_x)(P_x-\nu) \le \Phi(P_x) - \Phi(\nu), \quad \forall \nu \in \mathbb{R}_+, \tag{15}$$

the optimal points ν_1^* *and* ν_2^* *coincide and the optimal pdf is given by* $p^*_{\boldsymbol{w}}(\boldsymbol{w}) = \delta(\boldsymbol{w}-\boldsymbol{w}^*)$*, where* $\boldsymbol{w}^* = \boldsymbol{w}_1^* = \boldsymbol{w}_2^*$*.*

Proof: Please refer to Appendix VI. ∎

Proposition 3 reveals that there is an optimal transmit vector $\boldsymbol{x}$ which is discrete and characterized by scalar unit-norm symbols s with an arbitrary phase[4] and at most two beamforming vectors, $\boldsymbol{w}_1^*$ and $\boldsymbol{w}_2^*$. As in Corollary 1, these beamforming vectors coincide if inequality (15) holds.

We note that $\boldsymbol{w}_1^*$ and $\boldsymbol{w}_2^*$ in Proposition 3 are characterized by the values ν_1^* and ν_2^* obtained as solutions of the non-convex problems (9) and (10), respectively, that also can be solved using the grid-search method in Algorithm 1. However, unlike for MISO and SIMO systems, in order to obtain the value of $\Phi(\cdot)$ for a given transmit power value ν, the maximum value of $\Psi(\cdot)$ as solution of (14) is required. We note that (14) is a non-convex problem and, hence, obtaining its optimal solution is, in general, NP-hard. However, since problem (14) belongs to the class of monotonic optimization problems, in Section IV-C.1, we first obtain the optimal solution exploiting the polyblock outer optimization approach [29]. Then, in Section IV-C.2, for practical EH models satisfying Assumption 4, we propose an iterative low-complexity algorithm to obtain a suboptimal solution of the problem.

1) Optimal Solution: In the following, we obtain the optimal solution of non-convex problem (14) exploiting monotonic optimization [29]. To this end, similar to the monotonic polyblock optimization framework in [29], [33], we obtain the optimal solution of (14) by exploring the feasible set $\mathcal{V}$ of (14) determined by constraint $\|\boldsymbol{w}\|_2^2 = \nu$. First, we enclose $\mathcal{V}$ by constructing an initial polyblock $\mathcal{B}^{(1)}$ with an initial set of vertices $\mathcal{L}^{(1)} = \{\tilde{\boldsymbol{y}}_d^{(1)} | d \in \{1,2,\ldots,2^{2N^{\mathrm{T}}}\}\}$, where $\tilde{\boldsymbol{y}}_d^{(1)} \in \mathbb{C}^{N^{\mathrm{T}}}$ is a vector, whose k^{th} element is defined as $\tilde{y}_{d,k}^{(1)} = (-1)^{a_{n-1}^d}\nu + j(-1)^{a_n^d}\nu$. Here, $n = 2^k$ and $a_p^d \in \{0,1\}$ denotes bit p in the binary representation of number d, see Fig. 4(a). Then, since the objective function in (14) is monotonically increasing in $|\boldsymbol{w}|$, i.e., in $|w_1|, |w_2|, \ldots, |w_{N^{\mathrm{T}}}|$, in iteration $m \ge 1$ of the proposed algorithm, as shown in Fig. 4(b), we choose a vertex $\boldsymbol{y}^{(m)}$ from the set of vertices $\mathcal{L}^{(m)}$ that maximizes the objective function, i.e., $\boldsymbol{y}^{(m)} = \arg\max_{\boldsymbol{y}\in\mathcal{L}^{(m)}} \Psi(\boldsymbol{y})$. We calculate the intersection point $\psi^{(m)}$ between the feasible set $\mathcal{V}$ and the line that connects the origin and vertex $\boldsymbol{y}^{(m)}$ as $\boldsymbol{\chi}^{(m)} = \sqrt{\nu}\frac{\boldsymbol{y}^{(m)}}{\|\boldsymbol{y}^{(m)}\|_2}$. Then, based on vertex set $\mathcal{L}^{(m)}$, we generate a set of new vertices $\mathcal{L}_{\mathcal{B}}^{(m+1)} = \{\tilde{\boldsymbol{y}}_1^{(m+1)}, \tilde{\boldsymbol{y}}_2^{(m+1)}, \ldots, \tilde{\boldsymbol{y}}_{N^{\mathrm{T}}}^{(m+1)}\}$ and, thus, construct the new polybock $\mathcal{B}^{(m+1)}$ with vertex set $\mathcal{L}^{(m+1)} = \mathcal{L}^{(m)} \cup \mathcal{L}_{\mathcal{B}}^{(m+1)} \setminus \{\boldsymbol{y}^{(m)}\}$, see Fig. 4(c). This procedure is continued until the feasible set $\mathcal{V}$ is enclosed by the final polyblock $\mathcal{B}^{(1)} \supset \mathcal{B}^{(2)} \supset \cdots \supset \mathcal{V}$. Finally, as solution of (14), we select the vertex $\boldsymbol{\chi}^*$ that maximizes the objective function $\Psi(\boldsymbol{w})$. The proposed algorithm is summarized in Algorithm 2.

We note that the computational complexity of Algorithm 2 increases exponentially with the number of antennas N^{T} employed at the TX. Therefore, obtaining the optimal value of function $\Phi(\nu)$ may not be feasible in practical multi-user MIMO WPT systems. Nevertheless, the obtained optimal

[4]We note that the phase θ_s of scalar symbol s can be chosen arbitrarily in each time slot n. This degree of freedom can be further exploited, for example, for information transmission [24].

Algorithm 2 Polyblock Outer Approximation Algorithm

Initialize: Polyblock $\mathcal{B}^{(1)}$ with a vertex set $\mathcal{L}^{(1)}$, iteration index $m = 1$, vertex $\boldsymbol{y}^{(1)}$, and error tolerance ϵ_{PA}.

repeat

1. Construct a smaller polyblock $\mathcal{B}^{(m+1)}$ with vertex set $\mathcal{L}^{(m+1)}$ by replacing $\boldsymbol{y}^{(m)}$ with N^{T} new vertices $\mathcal{L}_{\mathcal{B}}^{(m+1)} = \{\tilde{\boldsymbol{y}}_1^{(m+1)}, \tilde{\boldsymbol{y}}_2^{(m+1)}, \ldots, \tilde{\boldsymbol{y}}_{N^{\text{T}}}^{(m+1)}\}$. The new vertex $\tilde{\boldsymbol{y}}_k^{(m+1)}$, $k \in \{1, 2, \ldots, N^{\text{T}}\}$, is given by

$$\tilde{\boldsymbol{y}}_k^{(m+1)} = \boldsymbol{y}^{(m)} - (y_k^{(m)} - x_k^{(m)})\boldsymbol{u}_k,$$

where $x_k^{(m)}$ is the k^{th} element of $\boldsymbol{\chi}^{(m)} = \sqrt{\nu}\frac{\boldsymbol{y}^{(m)}}{\|\boldsymbol{y}^{(m)}\|_2}$ and $\boldsymbol{u}_k$ is a unit vector containing only one non-zero element at position k.

2. Find $\boldsymbol{y}^{(m+1)} \in \mathcal{L}^{(m+1)}$ as the vertex that maximizes $\Psi(\boldsymbol{y})$, i.e.,

$$\boldsymbol{y}^{(m+1)} = \underset{\boldsymbol{y} \in \mathcal{L}^{(m+1)}}{\arg\max}\{\Psi(\boldsymbol{y})\}$$

3. Set $m = m + 1$

until $\frac{\|\boldsymbol{y}^{(m)} - \boldsymbol{\chi}^{(m)}\|_2}{\|\boldsymbol{y}^{(m)}\|_2} \leq \epsilon_{\text{PA}}$;

Output: $\boldsymbol{w}^* = \arg\max_{\boldsymbol{y} \in \{\boldsymbol{\chi}^{(1)}, \boldsymbol{\chi}^{(2)}, \ldots, \boldsymbol{\chi}^{(m-1)}\}} \Psi(\boldsymbol{y})$, $\Phi(\nu) = \Psi(\boldsymbol{w}^*)$

solution provides a performance upper-bound for any suboptimal scheme. In the next section, we propose an iterative low-complexity algorithm to obtain a suboptimal solution of (14).

2) Suboptimal Solution: In the following, we consider a practical EH model $\phi(\cdot)$ that satisfies Assumption 4. For this model, we propose an iterative low-complexity algorithm based on SDR and SCA to determine a suboptimal solution of (14). To this end, we first define matrix $\boldsymbol{W} = \boldsymbol{w}\boldsymbol{w}^H$ and reformulate problem (14) equivalently as follows:

$$\underset{\boldsymbol{W} \in \mathcal{S}_+}{\text{maximize}} \ \hat{\Psi}(\boldsymbol{W}) \tag{16a}$$

$$\text{subject to} \ \text{Tr}\{\boldsymbol{W}\} \leq \nu, \tag{16b}$$

$$\text{rank}\{\boldsymbol{W}\} = 1, \tag{16c}$$

where $\hat{\Psi}(\boldsymbol{W}) = \sum_{m=1}^{M}\sum_{p=1}^{N_m^{\text{E}}} \xi_m \phi(\boldsymbol{g}_p^m \boldsymbol{W} \boldsymbol{g}_p^{mH})$ and $\mathcal{S}_+$ denotes the set of positive semidefinite matrices. Since the objective function in (14) is monotonic non-decreasing in $|\boldsymbol{w}| = \{|\boldsymbol{w}_1|\,|\boldsymbol{w}_2|\ldots|\boldsymbol{w}_{N^{\text{T}}}|\}^\top$, we relax the equality constraint in (14) by inequality constraint (16b) [29].

Optimization problem (16) is non-convex due to the non-concavity of objective function (16a) and the non-convexity of constraint (16c). Therefore, in order to obtain a suboptimal solution of (16), we first eliminate constraint (16c). Then, we denote the total number of rectennas at the EH nodes by $K = \sum_{m=1}^{M} N_m^{\text{E}}$ and define the sets $\mathcal{W}_k, k \in \{0, 1, \ldots, K\}$, of matrices $\boldsymbol{W}$ such that $\forall \boldsymbol{W} \in \mathcal{W}_k$ exactly k rectifiers are driven into saturation. We note that $\mathcal{W}_1 \cup \mathcal{W}_2 \cup \cdots \cup \mathcal{W}_K = \mathcal{S}_+$. Furthermore, rectifier p of EH node m is driven into saturation if and only if $\boldsymbol{g}_p^m \boldsymbol{W} \boldsymbol{g}_p^{mH} \geq A_s^2$. Hence, set $\mathcal{W}_k, k \in \{0, 1, \ldots, K\}$, consists of $T_k = \frac{K!}{k!(K-k)!}$ convex subsets, where $k!$ denotes the factorial of k, i.e., $\mathcal{W}_k = \mathcal{W}_k^1 \cup \mathcal{W}_k^2 \cup \cdots \cup \mathcal{W}_k^{T_k}$. Each convex subset $\mathcal{W}_k^t, t \in \{1, 2, \ldots, T_k\}$, consists of all matrices $\boldsymbol{W}$ which drive into saturation a specific combination of k rectennas. We note that the objective function in (16) is convex for each of these subsets and, hence, applying SCA for solving (16) for $\boldsymbol{W} \in \mathcal{W}_k^t$, is promising [34], [35]. Thus, the solution of (16) can be obtained by exploring the subsets $\mathcal{W}_k^t, t \in \{1, 2, \ldots, T_k\}, k \in \{0, 1, \ldots, K\}$, and solving the resulting problem for each subset [1]. However, since the computational complexity of this exploration grows with $K!$, in the following, we obtain a suboptimal solution of (16).

For a given transmit power limit ν, we first determine a set of rectennas $\mathcal{W}^*$, which will be driven into saturation. To this end, we sort the channel gain vectors $\boldsymbol{g}_p^m$ in descending order of their norms as follows $\|\boldsymbol{g}_{p_1}^{m_1}\|_2 \geq \|\boldsymbol{g}_{p_2}^{m_2}\|_2 \geq \cdots \geq \|\boldsymbol{g}_{p_K}^{m_K}\|_2$, where $m_k \in \{1, 2, \ldots, M\}$, $p_k \in \{1, 2, \ldots, N_{m_k}^{\text{E}}\}$, and $k = 1, 2, \ldots, K$. Then, we check if it is possible to drive the k rectifiers with the best channel conditions, i.e., rectifier p_1 of EH node m_1, rectifier p_2 of EH node m_2, ..., rectifier p_k of EH node m_k, into saturation by solving the following optimization problem:

$$\underset{\boldsymbol{W} \in \mathcal{S}_+}{\text{maximize}} \ 1 \tag{17a}$$

$$\text{subject to} \ \boldsymbol{g}_{p_n}^{m_n} \boldsymbol{W} \boldsymbol{g}_{p_n}^{m_n H} \geq A_s^2, \quad \forall n \in \{1, 2, \ldots, k\}, \tag{17b}$$

$$\boldsymbol{g}_{p_{\tilde{n}}}^{m_{\tilde{n}}} \boldsymbol{W} \boldsymbol{g}_{p_{\tilde{n}}}^{m_{\tilde{n}} H} < A_s^2, \quad \forall \tilde{n} \in \{k+1, k+2, \ldots, K\}, \tag{17c}$$

$$\text{Tr}\{\boldsymbol{W}\} \leq \nu. \tag{17d}$$

Optimization problem (17) is convex and can be solved with standard numerical optimization tools, such as CVX [36]. Furthermore, although we dropped the rank-one constraint (16c), it can be shown that if (17) is feasible and $k > 0$, a beamforming matrix $\boldsymbol{W}_k^*$, which solves (17), has rank one. A corresponding proof is provided in the conference version [2, Appendix B] but is omitted here due to the space constraints. We denote by k^* the maximum number of rectifiers k, for which problem (17) is feasible. Note that if (17) is not feasible for any $k > 0$, we have $k^* = 0$. Then, we define the convex subset $\mathcal{W}^*$ that corresponds to the case, where the k^* rectifiers with the best channel conditions are driven into saturation. This set is given by

$$\begin{aligned}\mathcal{W}^* = \big\{&\boldsymbol{W} : \boldsymbol{W} \in \mathcal{S}_+, \\ &\boldsymbol{g}_{p_n}^{m_n} \boldsymbol{W} \boldsymbol{g}_{p_n}^{m_n H} \geq A_s^2, \forall n \in \{1, 2, \ldots, k^*\}, \\ &\boldsymbol{g}_{p_{\tilde{n}}}^{m_{\tilde{n}}} \boldsymbol{W} \boldsymbol{g}_{p_{\tilde{n}}}^{m_{\tilde{n}} H} < A_s^2, \forall \tilde{n} \in \{k^*+1, k^*+2, \ldots, K\}\big\}.\end{aligned} \tag{18}$$

Next, we reformulate problem (16) as follows:

$$\underset{\boldsymbol{W} \in \mathcal{W}^*}{\text{maximize}} \ \hat{\Psi}(\boldsymbol{W}) \quad \text{subject to} \ \text{Tr}\{\boldsymbol{W}\} \leq \nu. \tag{19}$$

Optimization problem (19) is still non-convex due to the non-concavity of the objective function. In the following,

TABLE I
OPTIMAL TRANSMIT STRATEGIES FOR MISO, SIMO, AND MIMO WPT SYSTEMS

	Optimal Transmit Strategies
MISO WPT	• Transmit symbol vector: $\boldsymbol{x} = \boldsymbol{w}s$, $s = r_s \exp(j\theta_s)$ • Beamforming: MRT $\boldsymbol{w} = \frac{\boldsymbol{g}^H}{\|\boldsymbol{g}\|_2}$ • Phase θ_s: May be chosen arbitrarily • Amplitude $r_s = \|s\|$: Discrete random variable with pdf $p^*_{r_s}(r_s)$ • The optimal pdf $p^*_{r_s}(r_s)$ is characterized in Proposition 1 and Corollary 3. • The computational complexity does not depend on N^{T}.
SIMO WPT	• Transmit symbol: $x = r_x \exp(j\theta_x)$ • Phase θ_x: May be chosen arbitrarily • Amplitude $r_x = \|x\|$: Discrete random variable with pdf $p^*_{r_x}(r_x)$ • The optimal pdf $p^*_{r_x}(r_x)$ is characterized in Proposition 2 and Corollary 4. • The computational complexity does not depend on M and $N^{\mathrm{E}}_m, m \in \{1, 2, \cdots, M\}$.
MIMO WPT	• Transmit symbol vector: $\boldsymbol{x} = \boldsymbol{w}s$, $s = \exp(j\theta_s)$ • Beamforming: Discrete random vector $\boldsymbol{w}$ with pdf $p^*_{\boldsymbol{w}}(\boldsymbol{w})$ • Phase θ_s: May be chosen arbitrarily • The optimal pdf $p^*_{\boldsymbol{w}}(\boldsymbol{w})$ is characterized in Proposition 3. • Vectors $\boldsymbol{w}_n, n \in \{1, 2\}$, in Proposition 3 are obtained with Algorithm 2 or Algorithm 3. • The computational complexity of one iteration of Algorithms 2 and 3 is exponential in N^{T} and polynomial in N^{T} and $K = \sum_{m=1}^{M} N^{\mathrm{E}}_m$, respectively.

we propose to solve (19) exploiting SCA [34]. To this end, we construct an underestimate of the objective function $\hat{\Psi}(\boldsymbol{W})$, which is convex in $\mathcal{W}^*$, as follows:

$$\hat{\Psi}(\boldsymbol{W}) \geq \hat{\Psi}(\boldsymbol{W}^{(t)}) + \mathrm{Tr}\{\nabla\hat{\Psi}(\boldsymbol{W}^{(t)})(\boldsymbol{W} - \boldsymbol{W}^{(t)})\}, \quad (20)$$

where $\boldsymbol{W}^{(t)}$ is the solution obtained in the iteration t of the algorithm and $\nabla\hat{\Psi}(\boldsymbol{W}^{(t)})$ denotes the gradient of $\hat{\Psi}(\boldsymbol{W})$ evaluated at $\boldsymbol{W}^{(t)}$. Thus, in each iteration t of the proposed algorithm, we solve the following optimization problem:

$$\begin{aligned} \boldsymbol{W}^{(t+1)} = \underset{\boldsymbol{W}\in\mathcal{W}^*}{\arg\max}\ & \hat{\Psi}(\boldsymbol{W}^{(t)}) \\ & + \mathrm{Tr}\{\nabla\hat{\Psi}(\boldsymbol{W}^{(t)})(\boldsymbol{W} - \boldsymbol{W}^{(t)})\} \quad (21a) \\ & \text{subject to}\ \ \mathrm{Tr}\{\boldsymbol{W}\} \leq \nu. \quad (21b) \end{aligned}$$

We note that (21) is a feasible convex optimization problem that can be solved with standard numerical optimization tools, such as CVX [36]. Furthermore, it can be shown that similarly to problem (17), the solution of (21) yields a matrix, whose rank is equal to one. Hence, we obtain the beamforming vector $\boldsymbol{w}^*$ as the dominant eigenvector of the solution $\boldsymbol{W}^*$ of (16) and compute the corresponding value of function $\Phi(\nu) = \Psi(\boldsymbol{w}^*)$. The proposed algorithm is summarized in Algorithm 3. We note that the proposed algorithm converges to a stationary point of (16) [35]. The computational complexity of a single iteration of the algorithm is polynomial and is given by[5] $\mathcal{O}(KN^{\mathrm{T}\frac{7}{2}} + K^2N^{\mathrm{T}\frac{5}{2}} + \sqrt{N^{\mathrm{T}}}K^3)$, where $\mathcal{O}(\cdot)$ is the big-O notation.

The optimal transmit strategies for MISO, SIMO, and MIMO WPT systems are summarized in Table I. We note that the computational complexities of the optimal transmit strategies for MISO and SIMO WPT systems are substantially lower than those of the optimal and suboptimal transmit strategies for MIMO WPT systems.

[5]The computational complexity of a convex semidefinite problem that involves an $n \times n$ positive semidefinite matrix and m constraints is given by $\mathcal{O}\big(\sqrt{n}(mn^3 + m^2n^2 + m^3)\big)$ [37]. Here, $n = N^{\mathrm{T}}$ and $m = K + 1$.

Algorithm 3 Suboptimal Algorithm for Solving Optimization Problem (14)

Initialize: Transmit power ν, tolerance error ϵ_{SCA}.

1. Sort the channel gain vectors by their norms $\big\|\boldsymbol{g}^{m_1}_{p_1}\big\|_2 \geq \big\|\boldsymbol{g}^{m_2}_{p_2}\big\|_2 \geq \cdots \geq \big\|\boldsymbol{g}^{m_K}_{p_K}\big\|_2$, where $K = \sum_{m=1}^{M} N^{\mathrm{E}}_m$, $m_k \in \{1, 2, \ldots, M\}$, $p_k \in \{1, 2, \ldots, N^{\mathrm{E}}_{m_n}\}$, and $k = 1, 2, \ldots, K$.

2. Set initial value $k^* = 0$.

for $j = 1$ to $K + 1$ **do**

3. Solve optimization problem (17) for $k = j$ and store $k^* = j$ if the problem is feasible

end

4. Determine set $\mathcal{W}^*$, set initial values $h^{(0)} = 0$ and $t = 0$, and randomly initialize $\boldsymbol{W}^{(0)}$.

repeat

a. For given $\boldsymbol{W}^{(t)}$, obtain $\boldsymbol{W}^{(t+1)}$ as the solution of (21)

b. Evaluate $h^{(t+1)} = \hat{\Psi}(\boldsymbol{W}^{(t+1)})$

c. Set $t = t + 1$

until $|h^{(t)} - h^{(t-1)}| \leq \epsilon_{\mathrm{SCA}}$;

5. Obtain $\boldsymbol{w}^*$ as the dominant eigenvector of $\boldsymbol{W}^{(t)}$ and evaluate $\Phi(\nu) = \Psi(\boldsymbol{w}^*)$

Output: $\Phi(\nu)$, $\boldsymbol{w}^*$

V. NUMERICAL RESULTS

In this section, we evaluate the performance of the proposed transmit strategies via simulations. First, we compare the performance of single-user MISO, SIMO, and MIMO

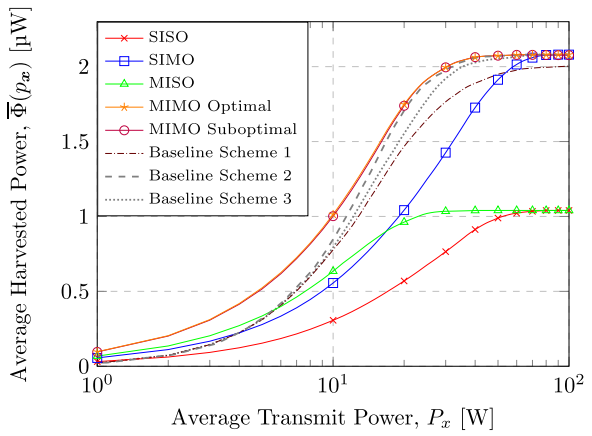

Fig. 5. Comparison of single-user SISO, SIMO, MISO, and MIMO WPT systems.

WPT systems. Then, we evaluate the performance of multi-user MIMO WPT systems for different numbers of antennas at the TX and EH nodes. Finally, we study the influence of the weights $\xi_m, m \in \{1, 2, \ldots, M\}$, associated with the EH nodes and determine the harvested power region.

A. Simulation Parameters

In the following, we provide the system parameters adopted in our simulations. In our simulations, the path losses are calculated as $35.3 + 37.6 \log_{10}(d_m)$, where d_m is the distance between the TX and EH node m [33]. Furthermore, in order to harvest a meaningful amount of power, we assume that the TX and each EH node have a line-of-sight link. Thus, the channel gains $\boldsymbol{g}_p^m$ follow Rician distributions with Rician factor 1 [38]. For the EH model $\phi(\cdot)$, we adopt the model proposed in [23] and given by (1) with parameter values $a = 1.29$, $B = 1.55 \cdot 10^3$, $I_s = 5$ μA, $R_L = 10$ kΩ, and $A_s^2 = 25$ μW. For Algorithms 1, 2, and 3 we adopt step size, grid size, and error tolerance values of $\Delta_\rho = 0.1$, $N_\rho = 10^3$, $\epsilon_{\text{PA}} = 10^{-3}$, and $\epsilon_{\text{SCA}} = 10^{-3}$, respectively. We note that the grid size N_ρ is chosen sufficiently large to ensure that the function $\Phi(\nu)$ saturates for $\nu = \rho_{N_\rho}$. The adopted simulation parameters are summarized in Table II. All simulation results were averaged over 1000 channel realizations.

B. Single-User WPT Systems

In this section, we investigate the performance of single-user WPT systems with different numbers of antennas at the TX and the EH node. The distance between the TX and the EH node is $d = 10$ m. The considered MISO and SIMO WPT systems employ $N^{\text{T}} = 2$ and $N^{\text{E}} = 2$ antennas at the TX and the EH node, respectively. For these systems, we evaluate the average harvested power $\overline{\Phi}(p_{\boldsymbol{x}}^*)$ for different values of the power budget P_x by applying Corollaries 3 and 4, respectively. In the considered single-user MIMO WPT system, the TX and EH nodes employ $N^{\text{T}} = N_1^{\text{E}} = 2$ antennas, respectively. For this system, optimal and suboptimal pdfs $p_{\boldsymbol{x}}(\boldsymbol{x})$ are determined by combining Algorithm 1 with Algorithms 2 and 3, respectively, and the values of $\overline{\Phi}(p_{\boldsymbol{x}}^*)$ are computed. For comparison, we also consider a SISO WPT system employing the optimal transmit strategy in [23]. As Baseline Scheme 1, we consider a MIMO WPT system with energy beamforming at the TX, which is optimal for linear EH nodes [6]. Furthermore, as Baseline Scheme 2, similar to [21], we consider a MIMO WPT system, where a scalar input symbol and a single beamforming vector are adopted at the TX. For this system, we obtain the optimal beamforming vector $\boldsymbol{w}^*$ as solution of (13) for $\nu = P_x$ with Algorithm 2 and compute the corresponding harvested power as $\overline{\Phi} = \Phi(\boldsymbol{w}^*)$. Finally, as Baseline Scheme 3, we consider a MIMO WPT system employing a single beamforming vector computed with the iterative algorithm proposed in [21] and based on the EH model in [18].

In Fig. 5, we plot the average harvested powers $\overline{\Phi}(p_{\boldsymbol{x}}^*)$ for different values of P_x. First, we observe that for each considered WPT setup, the average harvested power $\overline{\Phi}(\cdot)$ is bounded above, since for the EH model in (1), for sufficiently large values of P_x, all rectifiers of the EH node are driven into saturation. Furthermore, the saturation level of the harvested power is proportional to the number of rectennas employed at the EH node. As expected, the MIMO WPT system achieves a superior performance compared to the SIMO and MISO WPT systems, which, in turn, outperform the SISO WPT system significantly. Interestingly, the MISO WPT system can harvest more power than the SIMO WPT system if the transmit power budget at the TX is low, whereas, for large values of P_x, the single rectenna of the MISO WPT system is driven into saturation and, thus, more power can be harvested by the SIMO WPT system. Furthermore, we observe that for MIMO WPT systems, the proposed optimal transmit strategy, which employs two beamforming vectors, outperforms Baseline Schemes 1, 2, and 3, which utilize a single beamforming vector. This improvement is achieved at the expense of a higher computational complexity. Moreover, we observe that Baseline Scheme 2, which is based on the optimal beamforming vector obtained by Algorithm 2, outperforms Baseline Schemes 1 and 3, which employ the energy beamforming scheme in [6] and the iterative algorithm in [21], respectively. We note that the authors in [21] exploited the EH model derived in [18] and the breakdown effect of the rectifying diode is not taken into account in their iterative algorithm.

We observe that although the computational complexity of the proposed suboptimal scheme for obtaining the MIMO WPT beamforming vectors is significantly lower than that of the optimal scheme, the performances attained by both schemes are practically identical. Therefore, in the next section, to keep the computational complexity low, we adopt the proposed suboptimal scheme to evaluate the performance of multi-user MIMO WPT systems. Furthermore, since the analysis in [21] is limited to single-user MIMO WPT systems, we compare our schemes with Baseline Schemes 1 and 2 in the following sections.

C. Multi-User WPT Systems

In this section, we consider multi-user MIMO WPT systems, where the EH nodes are equipped with $N_m^{\text{E}} = 2$,

TABLE II
SIMULATION PARAMETERS

Parameters of the EH model	$a = 1.29$, $B = 1.55 \cdot 10^3$, $I_s = 5\,\mu\text{A}$, $R_L = 10\,\text{k}\Omega$, $A_s^2 = 25\,\mu\text{W}$	Distances between the TX and EH nodes	In Fig. 5: $d_1 = 10\,\text{m}$ In Fig. 6: $d_m = 10\,\text{m}, \forall m$ In Fig. 7: $d_1 = 10\,\text{m}$, $d_2 = 25\,\text{m}$
Step size in Algorithm 1 Grid size in Algorithm 1 Error tolerance in Algorithm 2 Error tolerance in Algorithm 3	$\Delta_\rho = 0.1$ $N_\rho = 10^3$ $\epsilon_{\text{PA}} = 10^{-3}$ $\epsilon_{\text{SCA}} = 10^{-3}$	Power budget at the TX	In Fig. 6: $P_x = 15\,\text{W}$ In Fig. 7(a): $P_x = 10\,\text{W}$ In Fig. 7(b): $P_x = 30\,\text{W}$

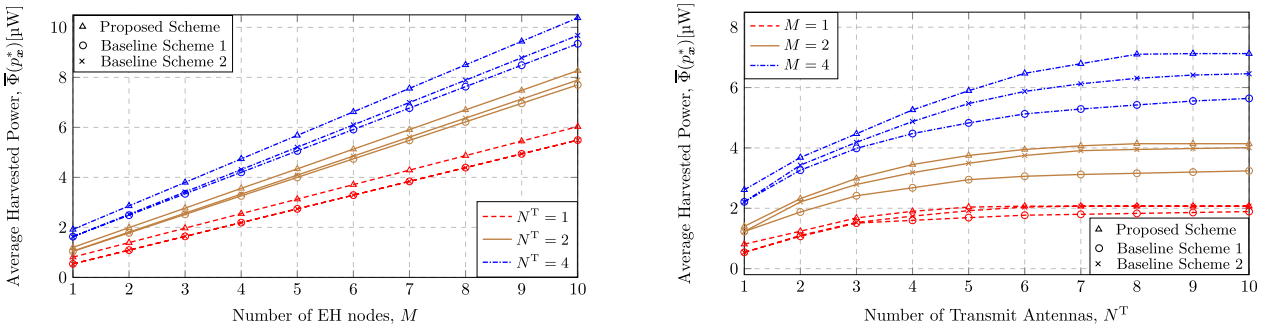

(a) Comparison for different numbers of EH nodes, M

(b) Comparison for different numbers of TX antennas, N^{T}

Fig. 6. Average harvested power $\overline{\Phi}(p_{\boldsymbol{x}}^*)$ for different numbers of transmit antennas N^{T} and EH nodes M.

$m \in \{1, 2, \ldots, M\}$, rectennas. In Fig. 6(a) and 6(b), we show the average harvested power for different numbers of transmit antennas N^{T} and EH nodes M, respectively. For each system setup, we compare the performance of the proposed transmit strategy with Baseline Scheme 1 and Baseline Scheme 2. The results in Fig. 6 are obtained assuming a transmit power budget of $P_x = 15$ W, equal weights for all EH nodes, i.e., $\xi_m = \frac{1}{M}$, and equal distances of $d_m = 10\,\text{m}, m = \{1, 2, \ldots, M\}$, between the TX and EH nodes. We observe that higher values of N^{T} and M yield larger average harvested powers $\overline{\Phi}$. Furthermore, we note that, similar to the single-user case, the proposed transmit strategy yields a better performance than the baseline schemes. Moreover, for SIMO WPT systems, i.e., for $N^{\text{T}} = 1$, the transmit strategies for Baseline Scheme 1 and Baseline Scheme 2 are identical and depend only on the power budget P_x. In Fig. 6(a), we observe that the harvested power depends practically linearly on the number of EH nodes. Although this result is relatively straightforward if the EH nodes are driven into saturation, see Fig. 5, Fig. 6(a) suggests that the linear growth of $\overline{\Phi}(\cdot)$ as M increases also holds when the rectifiers are not saturated. On the contrary, in Fig. 6(b), we observe that for a large number of transmit antennas, the average harvested power saturates since for the EH model in (1), the harvested power is bounded above. In fact, a larger number of transmit antennas N^{T} enables a more efficient exploitation of the transmit power budget, which yields a higher received power at the EH nodes. Furthermore, for larger M, the harvested power is distributed among a larger number of EH nodes and, thus, the number of transmit antennas needed to drive the rectennas into saturation, grows with M. We observe that for small numbers of the rectennas at the EH nodes, i.e., for $M = 1$ and $M = 2$, the saturation level of the average harvested power is nearly identical for the proposed scheme and Baseline Scheme 2, whereas, for Baseline Scheme 1, this saturation level is significantly lower. In fact, for massive MIMO systems, where the number of transmit antennas is much larger than the number of rectennas, the channel vectors $\boldsymbol{g}_p^m$ are practically orthogonal and, hence, the transmit strategy of Baseline Scheme 1 favors the rectenna with the best channel conditions while the powers transferred to the other rectennas are significantly lower [6], which may not be optimum in case of rectenna saturation.

Finally, in Fig. 7, we study the influence of weights ξ_m, $m \in \{1, 2\}$, for $M = 2$ EH nodes on the powers harvested by the individual EH nodes. For the results in Fig. 7, by varying the weights ξ_m, we determine the optimal transmit strategies that maximize the corresponding weighted sum of the average powers harvested at the EH nodes. Then, for the optimal pdfs $p_{\boldsymbol{x}}^*(\boldsymbol{x})$, we evaluate and plot the average harvested powers at the individual EH nodes, $\mathbb{E}_{\boldsymbol{x}}\{\psi_m(\boldsymbol{x})\}, m = \{1, 2\}$, respectively. For comparison, we also show the average harvested powers obtained with Baseline Scheme 1 and Baseline Scheme 2, respectively. In Fig. 7(a), we consider a low transmit power regime characterized by a power budget of $P_x = 10$ W, whereas for the results in Fig. 7(b), we assume a high transmit power regime with $P_x = 30$ W. The distances between the EH nodes and the TX are equal to $d_1 = 10$ m and $d_2 = 25$ m, respectively. In Fig. 7, we observe that higher values of N^{T} and P_x yield larger average harvested powers at both EH nodes. Furthermore, as expected, the proposed scheme yields a better performance compared to Baseline Scheme 1 and Baseline Scheme 2. For both transmit power regimes, we observe that for SIMO WPT, i.e., $N^{\text{T}} = 1$, the performances obtained with both baseline schemes are identical and do not depend on the adopted weights ξ_1 and ξ_2. In fact, in this case, the transmit strategies of the baseline

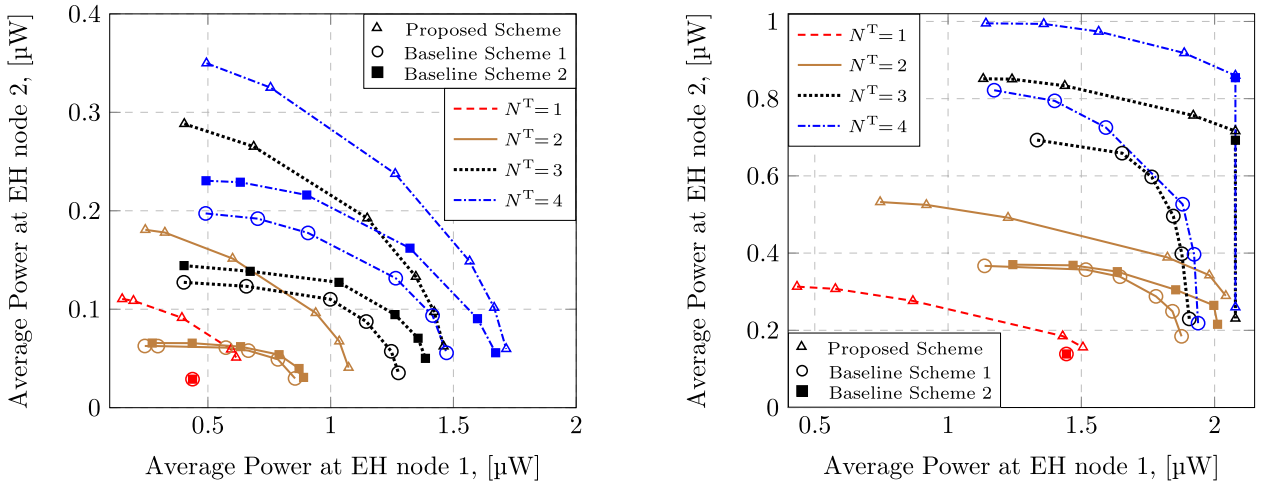

(a) Low transmit power regime, $P_x = 10$ W

(b) High transmit power regime, $P_x = 30$ W

Fig. 7. Harvested power regions of MIMO WPT system with $M = 2$ EH nodes equipped with $N_m^{\mathrm{E}} = 2, m = \{1, 2\}$, rectennas for different numbers of transmit antennas N^{T}.

schemes are identical and depend on the power budget P_x only. Moreover, in the high transmit power regime, we observe that the performance of Baseline Scheme 2 also does not depend on $\xi_m, m = \{1, 2\}$, for large numbers of transmit antennas, i.e., $N^{\mathrm{T}} = \{3, 4\}$, since, for large N^{T}, EH node 1 is driven into saturation anyways. However, for the other system setups, the choice of the weights $\xi_m, m \in \{1, 2\}$, enables a trade-off between the powers harvested at the EH nodes, which is characterized by a convex *harvested power region*. Furthermore, by increasing weight ξ_m, more power is harvested at EH node m at the expense of a reduction of the power harvested by the other node. Thus, by choosing the user weights, the TX can control the distribution of the harvested power among the users. In particular, for $\xi_1 = 1$ (and $\xi_2 = 0$), the TX maximizes the average harvested power at EH node 1 and neglects EH node 2, which may yield a substantial decrease of the power at EH node 2. In the high transmit power regime, EH node 1 is driven into saturation for $N^{\mathrm{T}} = \{3, 4\}$. In this case, by decreasing ξ_1 (and increasing ξ_2), it is possible to significantly increase the power harvested by EH node 2 without a substantial reduction of the power harvested by EH node 1.

VI. Conclusion

In this paper, we considered multi-user MIMO WPT systems with multiple EH nodes employing non-linear rectennas. Based on a set of assumptions, which are satisfied for practical EH circuits, we specified a general EH model. Then, we proposed an optimal transmit strategy that maximizes a weighted sum of the powers harvested at the EH nodes subject to a constraint on the power budget of the TX. For MISO WPT, we showed that transmission of scalar symbols with discrete random magnitudes, whose pdf has at most two mass points, via MRT beamforming is optimal. Next, for SIMO WPT, we proved that the optimal transmit symbol magnitude also has a discrete pdf with no more than two mass points. Then, for MIMO WPT, we showed that the optimal transmit strategy employs a scalar unit norm symbol and at most two beamforming vectors. In order to obtain these vectors, we formulated a non-convex optimization problem and presented optimal and suboptimal solutions. Our simulation results revealed that the proposed optimal and suboptimal schemes for MIMO WPT systems yield practically identical performances. Furthermore, we observed that the proposed MIMO WPT design achieves substantial performance gains compared to baseline schemes based on a linear EH model and a single beamforming vector. Moreover, for multi-user MIMO WPT systems, we showed that the harvested power saturates for large numbers of TX antennas. We also observed a trade-off between the powers harvested at individual EH nodes, which was characterized by a convex harvested power region.

Finally, the extension of the optimal MIMO WPT strategies presented in this paper to take into account non-idealities of practical communication systems, e.g., imperfect channel estimation [17], hardware impairments [16], [24], and peak power limitations at the TX [23], [24], is an interesting direction for future research.

Appendix A
Proof of Lemma 1

In the following, we prove Lemma 1. First, we note that since ν_2^* is the maximizer of the slope function $\sigma(\cdot, \cdot; f)$ for $\nu_1 = \nu_1^*$, then we have

$$\frac{f(\nu_2^*) - f(\nu_1^*)}{\nu_2^* - \nu_1^*} \geq \frac{f(\nu) - f(\nu_1^*)}{\nu - \nu_1^*}, \quad \forall \nu \geq \overline{\nu} \geq \nu_1^*. \tag{22}$$

Then, since ν_1^* is the minimizer of $\sigma(\cdot, \cdot; f)$ for $\nu_2 = \nu_2^*$, we have

$$\frac{f(\nu_2^*) - f(\nu_1^*)}{\nu_2^* - \nu_1^*} \leq \frac{f(\nu_2^*) - f(\nu)}{\nu_2^* - \nu}, \quad \forall \nu \leq \overline{\nu} \iff \tag{23}$$

$$f(\nu_1^*)\nu_2^* - f(\nu)(\nu_2^* - \nu_1^*) \geq f(\nu_2^*)(\nu_1^* - \nu) + f(\nu_1^*)\nu, \quad \forall \nu \leq \overline{\nu}. \tag{24}$$

Next, we subtract $f(\nu_1^*)\nu_1^*$ from both sides of (24). This allows us to rewrite both (22) and (24) as follows:

$$f(\nu_1^*) - f(\nu) \geq \frac{f(\nu_2^*) - f(\nu_1^*)}{\nu_2^* - \nu_1^*}(\nu_1^* - \nu), \tag{25}$$

respectively, which, thus, holds $\forall \nu \in \mathbb{R}$. Let us define linear function $g(\nu) = f(\nu_1^*) + \frac{f(\nu_2^*)-f(\nu_1^*)}{\nu_2^*-\nu_1^*}(\nu - \nu_1^*)$. Since, from (25), $g(\nu) \geq f(\nu)$, $\forall \nu \in \mathbb{R}$, then $\mathbb{E}_\nu\{f(\nu)\} \leq \mathbb{E}_\nu\{g(\nu)\} = g\big(\overline{\nu}\big) = f(\nu_1^*) + \alpha\big(f(\nu_2^*) - f(\nu_1^*)\big)$, where $\alpha = \frac{\overline{\nu}-\nu_1^*}{\nu_2^*-\nu_1^*}$. Finally, with $\alpha = 1-\beta$, we have $\mathbb{E}_\nu\{f(\nu)\} \leq \beta f(\nu_1^*) + (1-\beta) f(\nu_2^*)$, where the inequality holds with equality if the pdf of ν is given by $p_\nu^*(\nu) = \beta\delta(\nu - \nu_1^*) + (1-\beta)\delta(\nu - \nu_2^*)$. This concludes the proof.

Appendix B
Proof of Corollary 1

To prove this corollary, let us define a linear function $g(\nu) = f'(\overline{\nu})(\nu - \overline{\nu}) + f(\overline{\nu})$. We note that due to (7), $g(\nu) \geq f(\nu)$ $\forall \nu \in \mathbb{R}$. Thus, $\mathbb{E}_\nu\{f(\nu)\} \leq \mathbb{E}_\nu\{g(\nu)\} = g\big(\overline{\nu}\big)$, where the equality holds due to the linearity of $g(\nu)$. Hence, we conclude that the expectation of $f(\cdot)$ is upper-bounded by $\mathbb{E}_\nu\{f(\nu)\} \leq f(\overline{\nu})$, where the inequality holds with equality for pdf $p_\nu(\nu) = \delta(\nu - \overline{\nu})$. This concludes the proof.

Appendix C
Proof of Corollary 2

First, we note that the objective function in optimization problem (4) is monotonically non-decreasing, whereas the feasible set of the problem is defined by inequality $\mathbb{E}_\nu\{\nu\} \leq A_\nu$. Hence, (4) can be equivalently rewritten as follows [29]:

$$\underset{p_\nu}{\text{maximize}}\ \mathbb{E}_\nu\{f(\nu)\} \quad \text{subject to}\ \mathbb{E}_\nu\{\nu\} = A_\nu. \tag{26}$$

Therefore, if condition (7) holds for function $f(\nu)$ and $\overline{\nu} = A_\nu$, the objective function in (26) is upper-bounded by $\mathbb{E}_\nu\{f(\nu)\} \leq f(A_\nu)$, see Corollary 1, where the inequality holds with equality if $p_\nu(\nu) = \delta(\nu - A_\nu)$.

Let us now consider the case, where condition (7) does not hold for $f(\nu)$ and $\overline{\nu} = A_\nu$. In this case, the expectation of $f(\nu)$ is upper-bounded by (6), see Lemma 1, where the inequality holds with equality if the pdf of random variable ν is given by $p_\nu^*(\nu) = \beta\delta(\nu - \nu_1^*) + (1-\beta)\delta(\nu - \nu_2^*)$ with ν_1^*, ν_2^*, and β defined as in Lemma 1. This concludes the proof.

Appendix D
Proof of Proposition 1

We solve optimization problem (2) for a single-user MISO WPT system, i.e., $M = N_M^{\mathrm{E}} = 1$. First, let us consider a distribution of the transmit symbols $\boldsymbol{x}$ which has a point of increase at $\tilde{\boldsymbol{x}}_0$. For this distribution, a larger value of the input power at the EH node and, thus, an equal or larger value of $\overline{\Phi}(\cdot)$ can be attained by removing the mass point $\tilde{\boldsymbol{x}}_0$ and increasing the probability of symbol $\boldsymbol{x}_0 = \|\tilde{\boldsymbol{x}}_0\|_2 \frac{\boldsymbol{g}^H}{\|\boldsymbol{g}\|_2}\exp(j\theta_s)$ by the probability of symbol $\tilde{\boldsymbol{x}}_0$ of the former distribution, see Assumptions 3 [6]. We note that this transformation preserves the validity of the distribution, i.e., $\int p_{\boldsymbol{x}}(\boldsymbol{x})d\boldsymbol{x} = 1$, and, since the transmit powers for the two symbols are identical, i.e., $\|\tilde{\boldsymbol{x}}_0\|_2^2 = \|\boldsymbol{x}_0\|_2^2$, the new distribution does not affect the power budget of the TX.

Therefore, for the solution of (2), transmit vector $\boldsymbol{x} = \boldsymbol{w} r_s \exp(j\theta_s)$ is optimal, where $\boldsymbol{w} = \frac{\boldsymbol{g}^H}{\|\boldsymbol{g}\|_2}$ is the MRT beamformer and $r_s = |s|$ and θ_s are the magnitude and the arbitrary phase of random scalar symbol s, respectively. We denote the pdf of the transmit power values $\nu = r_s^2$, $\nu \in [0, +\infty)$, by $p_\nu(\nu)$. Then, the utility function in (3) can be rewritten as a function of pdf $p_\nu(\nu)$ as follows:

$$\begin{aligned}\overline{\Phi} &= \int_{\boldsymbol{x}} p_{\boldsymbol{x}}(\boldsymbol{x})\phi(|\boldsymbol{g}\boldsymbol{x}|^2)d\boldsymbol{x} = \int_{r_s} p_{r_s}(r_s)\phi(\|\boldsymbol{g}\|_2^2 r_s^2)dr_s \\ &= \int_\nu p_\nu(\nu)\Phi(\nu)d\nu = \mathbb{E}_\nu\{\Phi(\nu)\}.\end{aligned} \tag{27}$$

Hence, problem (2) can be equivalently rewritten as follows:

$$\underset{p_\nu}{\text{maximize}}\ \mathbb{E}_\nu\{\Phi(\nu)\} \quad \text{subject to}\ \mathbb{E}_\nu\{\nu\} \leq P_x. \tag{28}$$

Since optimization problem (28) is in the form of auxiliary problem (4), we obtain the solution by applying Corollary 2. First, the optimal pdf is given by $p_\nu^*(\nu) = \delta(\nu - P_x)$ if

$$\Phi'(P_x)(P_x - \nu) \leq \Phi(P_x) - \Phi(\nu), \quad \forall \nu \in \mathbb{R}_+. \tag{29}$$

We note that condition (29) is equivalent to (8). Furthermore, since $F_{r_s}(r_s) = F_\nu(r_s^2)$, where $F_{r_s}(r_s)$ and $F_\nu(\nu)$ are the cumulative density functions of r_s and ν, respectively, the optimal pdf of r_s is given by $p_{r_s}^*(r_s) = \delta(r_s - \sqrt{P_x})$.

If (29) does not hold, according to Corollary 2, the optimal solution of (28) is given by $p_\nu^*(\nu) = (1-\beta)\delta(\nu - \nu_1^*) + \beta\delta(\nu - \nu_2^*)$, where ν_1^* and ν_2^* are given by (9) and (10), respectively. Finally, since $F_{r_s}(r_s) = F_\nu(r_s^2)$, the equivalent optimal pdf of r_s is given by $p_{r_s}^* = (1-\beta)\delta(r_s - \sqrt{\nu_1^*}) + \beta\delta(r_s - \sqrt{\nu_2^*})$. This concludes the proof.

Appendix E
Proof of Proposition 2

In order to prove Proposition 2, we note that as a sum of non-decreasing functions, function $\Phi(\cdot)$ is also monotonically non-decreasing. Furthermore, the objective function can be equivalently rewritten as follows:

$$\begin{aligned}\overline{\Phi}(p_{r_x}) &= \int_{r_x} p_{r_x}(r_x)\Phi(r_x^2)dr_x \\ &= \int_\nu p_\nu(\nu)\Phi(\nu)d\nu = \mathbb{E}_\nu\{\Phi(\nu)\},\end{aligned} \tag{30}$$

where $p_\nu(\nu)$ is the pdf of the transmit power $\nu = r_x^2$.

Hence, for the considered SIMO WPT system, optimization problem (2) can be equivalently reformulated as follows:

$$\underset{p_\nu}{\text{maximize}}\ \mathbb{E}_\nu\{\Phi(\nu)\} \quad \text{subject to}\ \mathbb{E}_\nu\{\nu\} \leq P_x. \tag{31}$$

Since optimization problem (31) is in the form of auxiliary problem (4), the application of Corollary 2 yields Proposition 2. This concludes the proof.

APPENDIX F
PROOF OF COROLLARY 4

For the considered SIMO WPT systems with two rectennas, $\Phi(r_x^2) = \sum_{p=1}^{2} \phi(r_x^2|g_p|^2)$. Hence, the function $\Phi(\nu)$ is monotonic non-decreasing and convex in the intervals $[0, \rho_{\min})$, $[\rho_{\min}, \rho_{\max})$, and $[\rho_{\max}, \infty)$, respectively, and bounded $\Phi(\nu) \in [0, \Phi_r^{\max}]$, where $\Phi_r^{\max} = \Phi(\rho_{\max}) = 2\phi(A_s^2)$. Therefore, if affordable by the power budget constraint, i.e., $P_x \geq \rho_{\max}$, the optimal pdf is given by $p_r^*(r) = \delta(r - \sqrt{\rho_{\max}})$.

From the condition in Assumption 5, we obtain the following inequality:

$$\begin{aligned}\frac{\Phi(\rho_{\min})}{\rho_{\min}} &= \frac{\phi(A_s^2) + \phi(A_s^2\rho_{\min}/\rho_{\max})}{\nu_1} \\ &\geq \frac{\phi(A_s^2) + \phi(A_s^2)(\rho_{\min}/\rho_{\max})^2}{\rho_{\min}} \\ &= \frac{\phi(A_s^2)}{\rho_{\max}} \frac{\rho_{\max}^2 + \nu_1^2}{\rho_{\min}\rho_{\max}} \geq \frac{2\phi(A_s^2)}{\rho_{\max}} = \frac{\Phi(\rho_{\max})}{\rho_{\max}} > 0.\end{aligned} \tag{32}$$

Since function $\Phi(\cdot)$ is convex in the intervals $[0, \rho_{\min})$, $[\rho_{\min}, \rho_{\max})$ and $\frac{\Phi(\rho_{\min})}{\rho_{\min}} \geq \frac{\Phi(\rho_{\max})}{\rho_{\max}}$, the solution of the optimization problem in Proposition 2 is given by $\nu_1^* = 0$ and $\nu_2^* = \rho_{\min}$ if $P_x < \rho_{\min}$. Finally, we note that from (32), we have $\frac{\Phi(\rho_{\max})}{\rho_{\max}} \geq \frac{\Phi(\rho_{\max}) - \Phi(\rho_{\min})}{\rho_{\max} - \rho_{\min}}$ and, hence, if $P_x \in [\rho_{\min}, \rho_{\max})$, $\nu_1^* = \rho_{\min}$ and $\nu_2^* = \rho_{\max}$. This concludes the proof.

APPENDIX G
PROOF OF PROPOSITION 3

First, we note that for any arbitrary transmit symbol $\tilde{\boldsymbol{x}}$, there is a symbol $\hat{\boldsymbol{x}}$ given by

$$\hat{\boldsymbol{x}} = \arg\max_{\boldsymbol{x}} \Psi(\boldsymbol{x}) \quad \text{subject to } \|\boldsymbol{x}\|_2^2 = \|\tilde{\boldsymbol{x}}\|_2^2, \tag{33}$$

which has the same transmit power and yields a higher or equal value of $\Psi(\boldsymbol{x})$. Hence, for any arbitrary distribution of transmit symbols with a point of increase $\tilde{\boldsymbol{x}}$, a larger value of $\Psi(\boldsymbol{x})$ can be obtained by removing this point and increasing the probability of $\hat{\boldsymbol{x}}$ by the corresponding value.

Let us introduce now a function $\Phi(\nu)$ that returns the largest possible value of $\Psi(\boldsymbol{x})$ if a symbol with power ν was transmitted. This function is given by (14). We note that function $\Phi(\cdot)$ is monotonically non-decreasing, see Assumption 3. Then, the solution of (2) can be obtained by determining first the solution $p_\nu^*(\nu)$ of the following optimization problem:

$$\underset{p_\nu(\nu)}{\text{maximize}} \ \mathbb{E}_\nu\{\Phi(\nu)\} \quad \text{subject to } \mathbb{E}_\nu\{\nu\} \leq P_x. \tag{34}$$

Since (34) is in the form of (4), there exists an optimal discrete pdf $p_\nu^*(\nu)$ consisting of at most two mass points, ν_1^* and ν_2^*, see Corollary 2. Hence, the optimal symbol vector $\boldsymbol{x}$ can be decomposed as $\boldsymbol{x} = \boldsymbol{w}s$ with unit-norm symbols s and discrete random beamforming vector $\boldsymbol{w}$, whose pdf consists of at most two mass points evaluated as

$$\boldsymbol{w}_n^* = \underset{\boldsymbol{w} \,|\, \|\boldsymbol{w}\|_2^2 = \nu_n^*}{\arg\max} \ \Psi(\boldsymbol{w}),\ n \in \{1, 2\}, \tag{35}$$

with probabilities $p_{\boldsymbol{w}}^*(\boldsymbol{w}_n^*) = p_\nu^*(\nu_n^*)$, $n \in \{1, 2\}$, respectively. This concludes the proof.

REFERENCES

[1] N. Shanin, L. Cottatellucci, and R. Schober, "Harvested power region of two-user MISO WPT systems with non-linear EH nodes," 2021, *arXiv:2103.13802*.

[2] N. Shanin, L. Cottatellucci, and R. Schober, "Optimal transmit strategy for MIMO WPT systems with non-linear energy harvesting," in *Proc. 17th Int. Conf. Distrib. Comput. Sensor Syst. (DCOSS)*, Jul. 2021, pp. 520–527.

[3] I. F. Akyildiz, A. Kak, and S. Nie, "6G and beyond: The future of wireless communications systems," *IEEE Access*, vol. 8, pp. 133995–134030, 2020.

[4] B. Clerckx, R. Zhang, R. Schober, D. W. K. Ng, D. I. Kim, and H. V. Poor, "Fundamentals of wireless information and power transfer: From RF energy harvester models to signal and system designs," *IEEE J. Sel. Areas Commun.*, vol. 37, no. 1, pp. 4–33, Jan. 2019.

[5] P. Grover and A. Sahai, "Shannon meets Tesla: Wireless information and power transfer," in *Proc. IEEE ISIT*, Jul. 2010, pp. 2363–2367.

[6] R. Zhang and C. K. Ho, "MIMO broadcasting for simultaneous wireless information and power transfer," *IEEE Trans. Wireless Commun.*, vol. 12, no. 5, pp. 1989–2001, May 2013.

[7] R. Morsi, D. S. Michalopoulos, and R. Schober, "Performance analysis of near-optimal energy buffer aided wireless powered communication," *IEEE Trans. Wireless Commun.*, vol. 17, no. 2, pp. 863–881, Feb. 2018.

[8] X. Chen, C. Yuen, and Z. Zhang, "Wireless energy and information transfer tradeoff for limited-feedback multiantenna systems with energy beamforming," *IEEE Trans. Veh. Technol.*, vol. 63, no. 1, pp. 407–412, Jan. 2014.

[9] L. Liu, R. Zhang, and K.-C. Chua, "Multi-antenna wireless powered communication with energy beamforming," *IEEE Trans. Commun.*, vol. 62, no. 12, pp. 4349–4361, Dec. 2014.

[10] N. Sakai, K. Noguchi, and K. Itoh, "A 5.8-GHz band highly efficient 1-W rectenna with short-stub-connected high-impedance dipole antenna," *IEEE Trans. Microw. Theory Techn.*, vol. 69, no. 7, pp. 3558–3566, Jul. 2021.

[11] E. Boshkovska, D. W. K. Ng, N. Zlatanov, and R. Schober, "Practical non-linear energy harvesting model and resource allocation for SWIPT systems," *IEEE Commun. Lett.*, vol. 19, no. 12, pp. 2082–2085, Dec. 2015.

[12] J. Kim, B. Clerckx, and P. D. Mitcheson, "Signal and system design for wireless power transfer: Prototype, experiment and validation," *IEEE Trans. Wireless Commun.*, vol. 19, no. 11, pp. 7453–7469, Nov. 2020.

[13] K. Xiong, B. Wang, and K. J. R. Liu, "Rate-energy region of SWIPT for MIMO broadcasting under nonlinear energy harvesting model," *IEEE Trans. Wireless Commun.*, vol. 16, no. 8, pp. 5147–5161, Aug. 2017.

[14] G. Ma, J. Xu, Y. Zeng, and M. R. V. Moghadam, "A generic receiver architecture for MIMO wireless power transfer with nonlinear energy harvesting," *IEEE Signal Process. Lett.*, vol. 26, no. 2, pp. 312–316, Feb. 2019.

[15] E. Boshkovska, X. Chen, L. Dai, D. W. K. Ng, and R. Schober, "Max-min fair beamforming for SWIPT systems with non-linear EH model," in *Proc. IEEE 86th Veh. Technol. Conf. (VTC-Fall)*, Sep. 2017, pp. 1–6.

[16] E. Boshkovska, D. W. K. Ng, L. Dai, and R. Schober, "Power-efficient and secure WPCNs with hardware impairments and non-linear EH circuit," *IEEE Trans. Commun.*, vol. 66, no. 6, pp. 2642–2657, Jun. 2018.

[17] E. Boshkovska, D. W. K. Ng, N. Zlatanov, A. Koelpin, and R. Schober, "Robust resource allocation for MIMO wireless powered communication networks based on a non-linear EH model," *IEEE Trans. Commun.*, vol. 65, no. 5, pp. 1984–1999, May 2017.

[18] B. Clerckx and E. Bayguzina, "Waveform design for wireless power transfer," *IEEE Trans. Signal Process.*, vol. 64, no. 23, pp. 6313–6328, Dec. 2016.

[19] B. Clerckx, "Wireless information and power transfer: Nonlinearity, waveform design, and rate-energy tradeoff," *IEEE Trans. Signal Process.*, vol. 66, no. 4, pp. 847–862, Feb. 2018.

[20] Y. Huang and B. Clerckx, "Large-scale multiantenna multisine wireless power transfer," *IEEE Trans. Signal Process.*, vol. 65, no. 21, pp. 5812–5827, Nov. 2017.

[21] S. Shen and B. Clerckx, "Beamforming optimization for MIMO wireless power transfer with nonlinear energy harvesting: RF combining versus DC combining," *IEEE Trans. Wireless Commun.*, vol. 20, no. 1, pp. 199–213, Jan. 2021.

[22] Y. Huang and B. Clerckx, "Waveform design for wireless power transfer with limited feedback," *IEEE Trans. Wireless Commun.*, vol. 17, no. 1, pp. 415–429, Jan. 2018.

[23] R. Morsi, V. Jamali, A. Hagelauer, D. W. K. Ng, and R. Schober, "Conditional capacity and transmit signal design for SWIPT systems with multiple nonlinear energy harvesting receivers," *IEEE Trans. Commun.*, vol. 68, no. 1, pp. 582–601, Jan. 2020.
[24] N. Shanin, L. Cottatellucci, and R. Schober, "Markov decision process based design of SWIPT systems: Non-linear EH circuits, memory, and impedance mismatch," *IEEE Trans. Commun.*, vol. 69, no. 2, pp. 1259–1274, Feb. 2021.
[25] P. Horowitz and W. Hill, *The Art of Electronics*, 2nd ed. Cambridge, U.K.: Cambridge Univ. Press, 1989.
[26] U. Tietze and C. Schenk, *Advanced Electronic Circuits*. Berlin, Germany: Springer, 2012.
[27] L.-H. Lu, Y.-T. Liao, and C.-R. Wu, "A miniaturized Wilkinson power divider with CMOS active inductors," *IEEE Microw. Wireless Compon. Lett.*, vol. 15, no. 11, pp. 775–777, Nov. 2005.
[28] I. D. Coope and C. J. Price, "On the convergence of grid-based methods for unconstrained optimization," *SIAM J. Optim.*, vol. 11, no. 4, pp. 859–869, Jan. 2001.
[29] Y. J. Zhang, L. P. Qian, and J. Huang, "Monotonic optimization in communication and networking systems," *Found. Trends Netw.*, vol. 7, no. 1, pp. 1–75, Oct. 2013.
[30] R. Morsi, V. Jamali, D. W. K. Ng, and R. Schober, "On the capacity of SWIPT systems with a nonlinear energy harvesting circuit," in *Proc. IEEE Int. Conf. Commun. (ICC)*, May 2018, pp. 1–7.
[31] X. L. Polozec, *Input Impedance of Series Schottky Diode Detector Atlow and High Power*. Massy, France: Ericsson, May 2015, doi: 10.13140/RG.2.1.4530.9600. [Online]. Available: https://www.researchgate.net/publication/277323751_Input_Impedance_of_S%eries_Schottky_Diode_Detector_at_Low_and_High_Power
[32] S. P. Dokov and D. P. Morton, *Higher-Order Upper Bounds Expectation a Convex Function*. Berlin, Germany: Humboldt-Universität zu Berlin, Mathematisch-Naturwissenschaftliche Fakultät II, Institut Für Mathematik, 2002.
[33] W. R. Ghanem, V. Jamali, and R. Schober, "Resource allocation for secure multi-user downlink MISO-URLLC systems," in *Proc. IEEE Int. Conf. Commun. (ICC)*, Jun. 2020, pp. 1–7.
[34] Y. Sun, P. Babu, and D. P. Palomar, "Majorization-minimization algorithms in signal processing, communications, and machine learning," *IEEE Trans. Signal Process.*, vol. 65, no. 3, pp. 794–816, Feb. 2017.
[35] G. Lanckriet and B. K. Sriperumbudur, "On the convergence of the concave-convex procedure," in *Proc. Adv. Neural Inf. Process. Syst.*, vol. 22, Dec. 2009, pp. 1759–1767.
[36] M. Grant and S. Boyd. (2015). *CVX: MATLAB Software for Disciplined Convex Programming, Version 2.0 Beta (2013)*. [Online]. Available: http://cvxr.com/cvx.
[37] I. Pólik and T. Terlaky, *Interior Point Methods for Nonlinear Optimization*. Berlin, Germany: Springer, 2010.
[38] A. Goldsmith, *Wireless Communications*. Cambridge, U.K.: Cambridge Univ. Press, 2005.

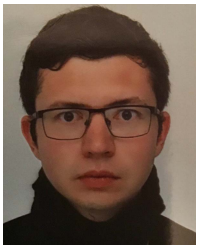

Nikita Shanin (Graduate Student Member, IEEE) received the Diploma degree from Bauman Moscow State Technical University (BMSTU), Moscow, Russia, in 2018. He is currently pursuing the Ph.D. degree with the Institute for Digital Communications, Friedrich-Alexander Universität (FAU) Erlangen-Nürnberg, Germany. His research interests fall into the broad areas of signal processing and wireless communications, including wireless information and power transfer.

Laura Cottatellucci (Member, IEEE) received the master's degree from La Sapienza University, Rome, Italy, the Ph.D. degree from the Technical University of Vienna, Austria, in 2006, and the Habilitation degree from the University of Nice-Sophia Antipolis, France. Since December 2017, she has been a Professor of digital communications at the Institute of Digital Communications, Friedrich Alexander Universität (FAU) Erlangen-Nürnberg, Germany, and has been an Adjunct Professor at EURECOM, France, since September 2021. From 1995 to 2000, she worked at Telecom Italia as responsible of industrial projects and as a Senior Researcher at Forschungszentrum Telekommunikation Wien, Austria, from April 2000 to September 2005. She was a Research Fellow at INRIA, France, from October 2005 to December 2005, and at the University of South Australia in 2006. From December 2006 to November 2017, she was also an Assistant Professor at EURECOM, France, where she was an Adjunct Professor from March 2018 to August 2019. Her research interests lie in the field of communications theory and signal processing for wireless communications, satellite, and complex networks. She has been an Elected Member of the IEEE Technical Committee on Signal Processing for Communications and Networking since 2017. She served as an Associate Editor for the IEEE TRANSACTIONS ON COMMUNICATIONS and the IEEE TRANSACTIONS ON SIGNAL PROCESSING from February 2016 to February 2020.

Robert Schober (Fellow, IEEE) received the Diploma (Univ.) and Ph.D. degrees in electrical engineering from the Friedrich-Alexander University (FAU) Erlangen-Nuremberg, Germany, in 1997 and 2000, respectively.

From 2002 to 2011, he was a Professor and the Canada Research Chair at the University of British Columbia (UBC), Vancouver, Canada. Since January 2012, he has been an Alexander von Humboldt Professor and the Chair of digital communication at FAU. His research interests fall into the broad areas of communication theory, wireless communications, and statistical signal processing. He received several awards for his work, including the 2002 Heinz Maier-Leibnitz Award of the German Science Foundation (DFG), the 2004 Innovations Award of the Vodafone Foundation for Research in Mobile Communications, the 2006 UBC Killam Research Prize, the 2007 Wilhelm Friedrich Bessel Research Award of the Alexander von Humboldt Foundation, the 2008 Charles McDowell Award for Excellence in Research from UBC, the 2011 Alexander von Humboldt Professorship, the 2012 NSERC E.W.R. Stacie Fellowship, and the 2017 Wireless Communications Recognition Award by the IEEE Wireless Communications Technical Committee. Since 2017, he has been listed as a Highly Cited Researcher by the Web of Science. He is a Fellow of the Canadian Academy of Engineering and the Engineering Institute of Canada. From 2012 to 2015, he served as the Editor-in-Chief of the IEEE TRANSACTIONS ON COMMUNICATIONS. Currently, he serves as a member of the Editorial Board for the PROCEEDINGS OF THE IEEE and as the VP Publications for the IEEE Communication Society (ComSoc).